Hydroclimate variability of western Thailand during the last 1400 years

Sakonvan Chawchai[a*], Guangxin Liu[b, c], Raphael Bissen[d], Denis Scholz[e], Dana F.C. Riechelmann[e], Hubert Vonhof[f], Regina Mertz-Kraus[e], Hong-Wei Chiang[c, g], Liangcheng Tan[h], Xianfeng Wang[c]

[a] *Morphology of Earth Surface and Advanced Geohazards in Southeast Asia Research Unit (MESA), Department of Geology, The Faculty of Science, Chulalongkorn University, Bangkok 10330, Thailand*

[b] *Research Center for Earth System Science, Yunnan University, Kunming 650500, China*

[c] *Earth Observatory of Singapore & Asian School of the Environment, Nanyang Technological University, Singapore 636798*

[d] *Department of Mining and Petroleum Engineering, Faculty of Engineering, Chulalongkorn University, Bangkok 10330, Thailand*

[e] *Institute for Geosciences, Johannes Gutenberg-University Mainz, 55099 Mainz, Germany*

[f] *Climate Geochemistry Department, Max Planck Institute for Chemistry, P.O. Box 3060, 55020, Mainz, Germany*

[g] *Department of Geosciences, National Taiwan University, Taipei 10617, Taiwan, ROC*

[h] *State Key Laboratory of Loess and Quaternary Geology, Institute of Earth Environment, Chinese Academy of Sciences, Xi'an 710075, China*

[*] *Corresponding author*: Dr. Sakonvan Chawchai (sakonvan.c@chula.ac.th) and Dr. Guangxin Liu (njuliuguangxin@gmail.com)

Abstract

Mainland Southeast Asia is located on the moisture transport route of the Indian summer monsoon (ISM) where hydroclimate records from speleothems have rarely been investigated. Here, we present a new multi-proxy ($\delta^{18}O$ and $\delta^{13}C$, trace elements, and grayscale) data set of stalagmite KPC1 from Khao Prae cave in western Thailand spanning most of the last 1400 years (500–1900 CE; CE, the Common Era). This multi-proxy data reveal a high variability between the wet and dry periods during 500–850 CE and 1150–1350 CE, a stable climate condition in 850–1150 CE, and an overall try trend since 1350 CE. The $\delta^{13}C$ values, trace elements concentrations, and grayscale values show centennial-scale fluctuations, which were probably driven by local hydrological process. In contrast, variations in the stalagmite $\delta^{18}O$ reflect integrated changes in rainfall amount from the ISM. In comparison with other Asian Monsoon

records for the last millennia, the KPC1 record agrees with the speleothem $\delta^{18}O$ records, as well as the lake multi-proxy and tree-ring PDSI data from Mainland Southeast Asia, but diverges from records from the Indo-Pacific equatorial regions and the western Pacific. We conclude that hydroclimate variability at the western side of Mainland Southeast Asia is mainly driven by changes in moisture transport of the ISM and modulated by expansion and contraction of the Intertropical convergent zone (ITCZ). However, the Pacific Walker Circulation (PWC) may have been the overriding control on precipitation on the eastern sides of Mainland Southeast Asia located close to the western Pacific. On socially relevant timescales, the KPC1 data set shows that a period of stable rainfall (850–1150 CE) coincides with the early success of the early empires (e.g. Pagan, Angkor, and Dai Viet) in Mainland Southeast Asia. In line with previous studies in the region, we speculate that the high variability in rainfall between 1150–1350 CE and droughts during 1350-1550 CE played a significant role in the demise of ancient societies in Southeast Asia.

Keywords: Stalagmite, Thailand, Southeast Asia, Indian summer monsoon, multi-proxy record

Highlights

- Stalagmite multi-proxy record of Thailand covering the last 1400 years.
- Unstable condition with long varying dry and wet phases during 500–850 CE and 1150-1350 CE.
- Stable rainfall in 850–1150 CE and dry conditions since 1350 CE.

1. Introduction

Mainland Southeast Asia is the continental part of Southeast Asia, including the countries of Myanmar, Thailand, peninsular Malaysia, Laos, Cambodia, and Vietnam. This region is bordered by the Indian Ocean in the west and the Pacific Ocean in the east. Mainland Southeast Asia is home to over 300 million people, who are highly reliant on farming. The regional social-economic health is, therefore, highly vulnerable to various hazards induced by hydroclimate changes, such as droughts and floods (Thirumalai et al., 2017; Waibel et al., 2018). The climate system in Mainland Southeast Asia is characterized by the interactions between different Asian monsoon subsystems [

the Indian summer monsoon (ISM), the East Asian summer monsoon (EASM), and the Western North Pacific monsoon (WNPM)] (Buckley et al., 2014). In addition, the regional hydroclimate is also modulated by the El Niño-Southern Oscillation (ENSO) (Mann and Jones, 2003; Räsänen et al., 2016; Singhrattna et al., 2005; Yamoah et al., 2016a), the Indian Ocean Dipole (IOD) (Ding et al., 2010; Ummenhofer et al., 2013), and the movement of the Intertropical convergent zone (ITCZ) (Chawchai et al., 2015; Tierney et al., 2010). Due to this complexity, our current understanding of hydroclimate changes in Southeast Asia is still limited. In addition, paleoclimatic records from the region are spatially unevenly distributed and the influence of climate mechanisms, such as the ITCZ (Denniston et al., 2016; Eroglu et al., 2016; Haug et al., 2001; Sachs et al., 2009; Yan et al., 2015), ENSO (Tan, 2016; Xu et al., 2019; Yan et al., 2011) and Pacific Decadal Oscillation (Cook et al., 2010; D'Arrigo and Ummenhofer, 2015), during historical times are controversially discussed. Therefore, robust temporal and spatial hydroclimate records from Mainland Southeast Asia are important, as they will allow evaluation of the climate forcing and help us to better understand the regional hydroclimate changes.

In recent years, stalagmites have provided robust hydroclimate information with precise age controls from ^{230}Th/U dating. Typical hydrological proxies used in stalagmite research are stable isotopes ($\delta^{18}O$ and $\delta^{13}C$) (Hendy, 1971; McDermott, 2004; Wong and Breecker, 2015), trace element concentrations (Fairchild et al., 2006; Fairchild and Treble, 2009a), and/or annual laminae (Baker et al., 2008; Shopov et al., 1994; Tan et al., 2006). For Asian monsoon regions, the observed changes in stalagmite $\delta^{18}O$ values and their relationship to the past hydroclimate appear to be different at each study site and are interpreted in various ways related to the monsoon timing, frequency, and strength (Caley et al., 2014; Li et al., 2019; Liu et al., 2015, 2014; Pausata et al., 2011a). The factors that control stalagmite $\delta^{18}O$ signals are still under considerable debates, such as changes in local or regional precipitation amounts (Berkelhammer et al., 2010; Sinha et al., 2011a), precipitation seasonality (Wang et al., 2001), atmospheric circulation (Chiang et al., 2015), and the degree of upstream rainout during transport (Pausata et al., 2011a; Wang et al., 2019).

Most speleothem studies that focused on the recent 2000 years are from China (Dykoski et al., 2005; Tan et al., 2017, 2011, 2009; Wang et al., 2005; Zhang et al., 2008), India (Denniston et al., 2000; Kathayat et al., 2017; Sinha et al., 2011a, 2011b, 2007), and Indonesia and Borneo, Malaysia (Griffiths et al., 2016; Partin et al., 2007;

Wurtzel et al., 2018). Stalagmite $\delta^{18}O$ values are generally interpreted as reflecting variations in precipitation amount and changes in monsoonal rainfall intensity. Stalagmite $\delta^{18}O$ records from China and India suggest a strong coupling between the Asian monsoon and climate variability in the Northern Hemisphere as well as potential links to changes in solar activity and/or oceanic and atmospheric circulation (e.g., Sinha et al., 2011a, 2011b; Zhang et al., 2008). However, modern precipitation data shows no significant correlation between sites that are hundreds of kilometers apart (Conroy and Overpeck, 2011; Dayem et al., 2010; Raghavan et al., 2018). A new speleothem $\delta^{18}O$ record from northern Laos (close to southern China) revealed changes in rainfall upstream and exhibited a positive correlation with solar activity (Wang et al., 2019). Whereas, the $\delta^{18}O$ records from equatorial regions (Flores Island and Sulawesi, Indonesia), suggest rainfall changes resulted from shifts in the ITCZ and the Pacific Walker circulation (PWC) (Griffiths et al., 2016; Krause et al., 2019). A recent stalagmite $\delta^{18}O$ record from Klang cave on the Thai-Malay peninsula, between the tropics and higher latitudes of Mainland Southeast Asia, suggested that both the ITCZ and the ENSO have influenced rainfall variability in this region (Tan et al., 2019).

Few speleothem studies from Southeast Asia have focused on additional proxies, such as $\delta^{13}C$ values and trace element concentrations. Recent studies from southern China and Laos reported that changes in speleothem $\delta^{13}C$ values were associated with regional hydrological changes (Liu et al., 2016; Wang et al., 2019). Hence, multi-proxy records preserved in speleothems can add valuable hydroclimate information for this region.

Western Thailand (Fig. 1A, B) is in the path of the ISM where moisture is sourced from the Bay of Bengal. In this region, paleoenvironmental and paleoclimatic records, especially those from stalagmites, have rarely been investigated so far (Cai et al., 2010; Chawchai et al., 2018; Muangsong et al., 2014). The scarcity of these studies limits the understanding of the spatial variability of the Asian summer monsoon. Here, we present a new stalagmite multi-proxy hydroclimate record ($\delta^{18}O$ and $\delta^{13}C$ values, trace element concentrations, and gray scale values) from Khao Prae cave, western Thailand, covering the last 1,400 years. Multi-proxy data sets can provide a robust base for discussing the response of different proxies used to infer hydroclimate conditions, regional patterns, and leads or lags in response to past rainfall variability. Our record can, therefore, provide important information for discussing potential forcing mechanisms of the monsoon in Southeast Asia and facilitate the construction of a

synchronized historical narrative for mainland Southeast Asia.

2. Cave and Climate Settings

Khao Prae cave (15°05′ N, 99° 25' E; 420 m above mean sea level) is in Uthai Thani province, approximately 240 km northwest of Bangkok and about 160 km from the Andaman coast (Fig. 1B). The host rock of this cave is argillaceous Ordovician limestone (Department of Mineral Resources (DMR), 2009). The vegetation is quite dense and the soil thickness above the cave is about 1 m. The cave has only one entrance, and the main passage is approximately 200 m long. Stalagmite KPC1 was collected in a chamber about 100 m from the cave entrance. Air temperature inside the cave, recorded from January to December 2017, was quite stable and ranged from 23.5–25.2 °C with a relative humidity of > 97 % (supplementary data Table1).

The study site is mainly influenced by the southwest ISM (Fig. 1A, B), with 105–110 rainy days and a mean annual precipitation of 1100–1200 mm. Maximum and minimum temperatures between 1951–2016 were 34.4 °C (April) and 20.2 °C (December), respectively, (Thai Meteorological Department; TMD). During the rainy season (May to October), the summer monsoon delivers about 80 % of the annual rainfall with a peak precipitation of 240 mm in September (Fig. 1C). From the records of the last 68 years, tropical cyclones from the South China Sea contribute additional precipitation, particularly during September and October (TMD). The northeast (NE) winter monsoon causes dry conditions between November and April (Fig. 1C).

3. Material and Methods

3.1 X-ray computed tomography (CT scan) and gray scale values

Sample KPC1 had a nearly symmetrical candle shape with a length of 20.6 cm and a diameter of 6–8 cm. The outer surface was smooth and showed no indication of dissolution features. Before cutting, KPC1 was subjected to a CT scan (GE Discovery 750 HD) (Fig. 2A) at King Chulalongkorn Memorial Hospital, Bangkok, Thailand. The CT instrument was operated at a tube voltage of 140 kV and a current intensity of 80 mA with the scanner was set to a 0.625 mm slice thickness and a 0.4 mm overlay between slice spaces. Reconstructed images were exported as Digital Imaging and Communications in Medicine (DICOM) files. CT image processing and data analysis were performed using MeVisLab software (ver. 2.6.2). The CT image is shown in grayscale images of axial sections in Fig. 2A, which indicate the stalagmite's density;

171 the denser the scanned stalagmites, the brighter the images and vice versa. The CT scan
172 technique has previously been used in studying speleothem features, including porosity
173 (Mickler et al., 2004), macro-holes and post-depositional off axis holes (Zisu et al.,
174 2012), calcite density (Vanghi et al., 2015; Walczak et al., 2015), and indication of
175 diagenesis in speleothems (Bajo et al., 2016). In this study, the visualization of the CT
176 image grayscale was used for selecting cutting sections before proxy analysis.
177 The cut and polished section of the stalagmite was scanned using a high-
178 resolution scanner (Microtek, RGB/3200dpi; Fig. 2B). The laminae gray scale values
179 were measured using the IMAGEJ software (https://imagej.net/Welcome). The gray
180 scale values are obtained from the average values, which were calculated using the
181 intensities of red (R), green (G), and blue (B) light. The gray scale values were set range
182 from 0 (black) to 250 (white).
183
184 **3.2 ^{230}Th/U dating**
185 Age control for stalagmite KPC1 was based on eighteen ^{230}Th/U ages (Table 1),
186 for which subsamples were drilled along the growth axes (Fig. 3A). Procedures for U
187 and Th chemical separation and purification were similar to those previously described
188 in Chiang et al. (2019), Edwards et al. (1986), and Shen et al. (2012), in a class-1000
189 chemistry cleanroom at the Earth Observatory of Singapore (EOS), Nanyang
190 Technological University (NTU) of Singapore. The U and Th isotopic ratios were
191 measured by a Thermo Scientific Neptune Plus multi-collector inductively coupled
192 plasma mass spectrometer (MC-ICP-MS) in the Environmental Geochemistry
193 Laboratory at EOS. Intensities of all the uranium and thorium isotopes were measured
194 with a peak-jumping protocol on a secondary electron multiplier equipped with a
195 retarding potential quadrupole lens to improve abundance sensitivity, except for those
196 of ^{238}U and ^{232}Th, which were measured on Faraday cups. The ^{230}Th/U dating results
197 are summarized in Table 1. All the uncertainties are presented at the 2σ level or two
198 standard deviations of the mean ($2\sigma_m$) unless otherwise noted. Ages are given in
199 thousands of years before present (ka BP; where "present" is defined as CE 1950). Two
200 age models (Fig. 3B, C) were constructed using the StalAge (Scholz and Hoffmann,
201 2011) and BACON (Blaauw and Christen, 2011) age models.
202
203 **3.3 Trace elements composition and X-ray diffraction (XRD) analysis**
204 Elemental abundances were determined by laser ablation (LA)- ICP-MS, at the

Institute for Geosciences, Johannes Gutenberg University Mainz, Germany, using an ESI NWR193 ArF excimer LA system equipped with the TwoVol^2 ablation cell, operating at 193 nm wavelength, coupled to an Agilent 7500ce quadrupole ICP-MS. Ablation was performed in the line scan mode and surfaces were pre-ablated prior to each line scan to prevent potential surface contamination. Line scans (Fig. 4A) were performed at a scan speed of 10 µm/s, using a spot size of 110 µm and a laser repetition rate of 10 Hz. Laser energy on the samples was about 3 J/cm^2. Measured ion intensities were monitored in time-resolved mode and background intensities were measured for 15 s. Synthetic glass NIST SRM 612 was used to calibrate element concentrations applying the preferred values given in the GeoReM database (http://georem.mpch-mainz.gwdg.de/, application version 18; Jochum et al., 2011, 2005).

Quality control materials (QCMs) (USGS MACS-3 and USGS BCR-2G) were used to monitor the accuracy and precision of the LA-ICP-MS analysis and calibration strategy. Raw data were processed using TERMITE (Mischel et al., 2017), an R script for data reduction. ^{43}Ca was used as an internal standard and applied at a sample Ca concentration of 390,000 µg/g and the values reported in the GeoReM data base for the QCMs. Element concentrations determined for the QCMs mostly agreed within 15 % of the published values for USGS MACS-3 (Jochum et al., 2012) and the preferred values of the GeoReM database for USGS BCR-2G, and had a precision of < 0.02 % (1 relative standard deviation; R.S.D.). For data processing, principal component analysis (PCA) was performed to identify of variables whose behavior was similar and so controlled by the same process.

For mineralogical determination, eight selected dark layers (Fig. 2B) were drilled and ground for XRD (Bruker model D8 advance) analysis at the Department of Geology, Chulalongkorn University. The sample scans were run from 5–50° 2θ with 0.01 steps of 1 second/step scan. To identify the mineral composition, Bruker's EVA software was used.

3.4 Stable Isotope Ratios

The oxygen (δ^{18}O) and carbon (δ^{13}C) isotope profiles for KPC1 were based on 150 measurements (1 mm resolution; 15 cm from the top) of transect drilled parallel to the trace elements analysis (distance ≤ 5 mm) (Fig. 4A). Stalagmite KPC1 was drilled using a New Wave Research MicroMill following the protocol of Dettman and Lohmann (1995) and samples were analyzed with a Thermo Delta V mass spectrometer

equipped with a GASBENCH II preparation device at the Max Planck Institute for Chemistry, Mainz, Germany. Isotope ratios are reported as $\delta^{13}C$ and $\delta^{18}O$ values relative to Vienna Peedee Belemnite (VPDB). The reproducibility of a routinely analyzed lab $CaCO_3$ reference material was better than 0.1‰ for both $\delta^{18}O$ and $\delta^{13}C$ values (1standard deviation; S.D.).

4. Results

4.1 Chronology

The results of $^{230}Th/U$-dating are shown in Table 1. ^{238}U concentrations range from 100 to 500 ng/g, and ^{232}Th concentrations range from a few ng/g to tens of ng/g. The $^{230}Th/^{232}Th$ atomic ratios range from 3 to 26 x 10^{-6}. Generally, if the $^{230}Th/^{232}Th$ atomic ratios are larger than 1 x 10^{-3} (or $^{230}Th/^{232}Th$ activity ratios to be larger than ~200), the contribution of initial detrital ^{230}Th is considered insignificant (Richards and Dorale, 2003). However, for KPC1, the low $^{230}Th/^{232}Th$ atomic ratios, which result largely from high ^{232}Th concentrations and the young age of the samples, require a careful correction of the initial detrital ^{230}Th. Indeed, the uncorrected ages are not in a stratigraphic order, and those containing high ^{232}Th concentrations are apparently "older", indicating significant detrital contamination.

The common *a priori* estimation of the initial $^{230}Th/^{232}Th$ atomic ratio is 4.4 x 10^{-6} (Wedepohl, 1995), the value for a material at secular equilibrium assuming a $^{232}Th/^{238}U$ weight ratio of 3.8, based upon a tonalitic composition of the bulk continental crust with Th and U concentrations of 6.4 μg/g and 1.7 μg/g, respectively. However, such a value is clearly too high for KPC1, because the initial $^{230}Th/^{232}Th$ atomic ratio should be smaller than the smallest measured $^{230}Th/^{232}Th$ atomic ratio (3.1 ± 0.1 x 10^{-6}).

In this study, we re-calculated the initial $^{230}Th/^{232}Th$ atomic ratio for KPC1 to be 2.7 x 10^{-6}, based on the assumption that the ages of two subsamples at 1.5 mm distance from the top must be equal. Following this reasonable assumption, we then assign the commonly used value of 50% to the uncertainty of the calculated initial $^{230}Th/^{232}Th$ atomic ratio (i.e. 2.7 ± 1.4 x 10^{-6}). We consider the calculation robust, because most of the corrected ages are in a stratigraphic order within their age uncertainties (Hellstrom, 2006). Four corrected ages at 87, 135 and 185 mm, respectively (Table 1), have large uncertainties and are even not in stratigraphic order.

Therefore, these dates were excluded from the final age model.

Age-depth models were constructed using both the StalAge and BACON age models (Fig. 3B, C). The blue shapes show the dates with two standard deviations, the green line indicates the most likely age model, and the red lines show the 95 % confidence limits of the age models (Fig. 3B and C). StalAge and BACON gave similar results, which show that the conclusions of this study are not sensitive to the choice of the specific age model. Herein, we report the ages derived from the BACON age model.

The KPC1 record spans the period between 500 BCE and 1900 CE. Based on the physical properties of the stalagmite and chronological uncertainty, we therefore focus the further interpretation on the top 15 cm of the stalagmite (c. 500–1900 CE), which is above a possible hiatus, visible by a less dense layer in the CT image (arrow in Fig. 2A) and a porous and white layer in the scan picture (arrow in Fig. 2B).

4.2 Multi-Proxies

The CT images are displayed in grayscale (Fig. 2A), where lower densities are observed in areas with a high porosity, between 15 and 16 cm from the top of KPC1 (Fig. 2A). There is little variation in the CT scan numbers except for distinctly lower values at 15.6 cm. The cut and polished sample (Fig. 2B) show growth layers with distinctly darker bands interlayered with lighter bands. Small cavities are observed at the bottom of the sample, between 15.8 and 15.6 cm, and at 6.8 and at 5.8 cm from the top (Fig. 2B). The gray scale values range from 34–237 with a mean value of 127 (S.D. = 25). Darker layers exhibit lower gray scale values (< 100). These alternate with intervals of higher gray scale values (brighter color layers) (Fig. 4A, B).

The XRD data indicate that KPC1 is composed of calcite. For trace element composition, nine elements were monitored (Mg, Sr, Ba, Pb, Al, Mn, Fe, Cu, and Zn). Each elemental profile is plotted and visually compared with each other, and then PCA is performed (Supplementary Fig. S1). The commonly investigated elements Mg, Sr, Ba display low correlation and the concentrations of Pb and Al are mostly below detection limits. While the elemental profiles of Fe, Mn, Cu and Zn show similar patterns (Fig. 4C–F) with a correlation of $R^2 > 0.6$ (n =46,538). Higher elemental concentrations (Fe, Mn and Zn) are observed with lower gray scale values/darker colored layers (Fig. 4).

The $\delta^{13}C$ values of KPC1 ranged from -12.4 to -8.7 ‰ with a mean value of -10.4 ‰ (S.D. = 0.8‰; Fig. 5C). Lower $\delta^{13}C$ values are observed in some layers with

higher trace element concentrations during 500–850 CE and ~1150–1250 CE (Fig. 5A–C). The $\delta^{13}C$ values show oscillation around a long-term mean with centennial-scale variations and a millennium-long negative trend from 500–1250 CE, and positive trend from ~1350 to 1900 CE. The KPC1 $\delta^{18}O$ values range from -7.5 to -11.9 ‰ with a mean value of -9.2 ‰ (S.D. = 0.8‰; Fig 5D). The $\delta^{18}O$ values exhibit centennial-scale fluctuations with large amplitude changes observed during 500–850 CE and 1150–1350 CE (Fig. 5D).

5. Discussions

5.1 Interpretation of paleoclimate proxies

Trace elements, gray scale values and Stalagmite $\delta^{13}C$

Trace elements in speleothems can be transported from particles, colloids, and solutes in karstic waters (Fairchild and Treble, 2009a). For KPC1, a strong correlation ($R^2 > 0.6$) among trace elements (Fe, Mn, Cu, and Zn) suggests that one main geochemical process has a first-order control on these elements. In contrast to the solution-preference of divalent cations, metal elements (Fe, Mn, Cu, and Zn) have a tendency to show a strong sorption behavior in soils and organic ligands (Blaser et al., 2000; Hartland and Zitoun, 2018). Higher concentrations of such elements in speleothems would be expected in water associated with transport of organic molecules, colloidal and particle phases during periods of strong water flow/stronger rainfall (Borsato et al., 2007; Fairchild and Treble, 2009b; Zhou et al., 2008). Thus, the elemental peaks in the dark colored layers of KPC1 (Fig. 4) likely reflect stronger rainfall at the cave site.

Several studies indicate that speleothem $\delta^{13}C$ are controlled by local processes at cave sites, such as changes in local hydrology, soil activity, vegetation density and composition, and effective infiltration (Baker et al., 1997; Breitenbach et al., 2015; Fairchild and Treble, 2009b; Fohlmeister et al., 2011). For the darker layers of KPC1, we observe a negative correlation between $\delta^{13}C$ and the trace elements compositions (lower $\delta^{13}C$ values, higher trace element concentrations). Previous studies have suggested that stronger rainfall conditions enhance vegetation density and soil microbial productivity can lead to lower stalagmite $\delta^{13}C$ values (Cheng et al., 2016; Deininger et al., 2012; Fohlmeister et al., 2011; Tan et al., 2015). Both the high trace

elements and lower $\delta^{13}C$ values observed in the KPC1 darker layers suggest strong rainfall. Therefore, the trace elements and $\delta^{13}C$ records of KPC1 suggest high variability and frequent pluvial events between 500–850 and 1150–1250 CE.

Climatic significance of $\delta^{18}O$

It is important to test whether speleothem carbonate is deposited under isotopic equilibrium conditions before attempting any climatic interpretation of stalagmite $\delta^{18}O$. We first calculated the correlation factors (R^2) between $\delta^{18}O$ and $\delta^{13}C$ for KPC1 (Supplementary data Fig. S2); the correlation factor (R^2 = 0.27) argues against disequilibrium driven isotope fractionation during speleothem growth (Hendy, 1971). We further calculated rainfall $\delta^{18}O$ from the near-modern portion of speleothem $\delta^{18}O$ (~-9‰ VPDB, Fig. 5), using the equation provide by O'Neil et al. (1969), and an annual mean cave temperature of 24.3 °C. The calculated rainfall $\delta^{18}O$ (~ -6.9‰ VSMOW) is in an agreement with amount-weighted annual rainfall $\delta^{18}O$ near the cave site (~ -6.6 ‰ VSMOW; Fig. 6A), which further suggests that KPC1 was deposited under isotopic equilibrium conditions, with particularly the near-modern speleothem $\delta^{18}O$ values being robust.

The variations of KPC1 $\delta^{18}O$, therefore, capture the variations of $\delta^{18}O$ in the rainfall above the cave, and cave temperature. Considering that the temperature changes are likely to be within 1 °C during the growth period of KPC1 (Moberg et al., 2005), with a small temperature-dependent fractionation factor of ~ 0.25‰/°C, (O'Neil et al., 1969), we conclude that the KPC1 $\delta^{18}O$ changes (~ 2–4‰) largely result from the variations in the rainfall $\delta^{18}O$ at the cave site.

The $\delta^{18}O$ inferred from speleothems in Asian monsoon regions is commonly interpreted as an indicator of the monsoon intensity through a variety of proposed mechanisms, with lower $\delta^{18}O$ values reflecting wetter conditions/stronger monsoon and higher values reflecting drier conditions/weaker monsoon (Cheng et al., 2016; Dykoski et al., 2005; Sinha et al., 2011a; Wang, 2001; Zhang et al., 2008). Such interpretation, however, is subject to severe debates (Beck et al., 2018; Caley et al., 2014; Clemens et al., 2010; Liu et al., 2014; Pausata et al., 2011b). Therefore, a better understanding of speleothem $\delta^{18}O$ requires the examination of the rainfall $\delta^{18}O$ under the present day climate (Breitenbach et al., 2010; Dayem et al., 2010; Johnson and Ingram, 2004; Ruan et al., 2019).

Here, we analyzed a 2-year time series of monthly rainfall $\delta^{18}O$ values ($\delta^{18}O_p$) between 2016 and 2017 from Uthai Thani province (approximately 50 km from the study site). The data show a broadly negative correlation between the monthly mean $\delta^{18}O_p$ values and rainfall amount (Fig. 6A; R^2 = -0.71, P = 12, S.D. = 0.1‰), in accordance with a recent study in the region (Tan et al., 2019), suggesting that the local "amount effect" (Dansgaard, 1964) plays a crucial role in the rainfall $\delta^{18}O$ values.

In addition to the local rainfall amount, changes in the rainout prior to the region or the upstream "amount effect" may also influence the local rainfall $\delta^{18}O$ (Raghavan et al., 2018; Wei et al., 2018; Yang et al., 2016). We, therefore, further evaluated the contributions from different moisture sources by analyzing local rainfall $\delta^{18}O$ values ($\delta^{18}O_p$) together with air mass back-trajectories retrieved from NOAA's Hybrid Single Particle Langarian Integrated Trajectory (HYSPLIT4) model with the NCAR/NCEP Reanalysis 2.5 deg gridded data set. We calculated 6-day back trajectories daily from the site at 15°05' N, 99°25' E for the period from 2000–2009 (Fig. 6B). The rain-bearing trajectories (> 8.5 mm/day) were then selected based on rainfall amounts derived from the ERA-Interim data downloaded from the European Centre for Medium-Range Weather Forecasts public datasets and clustered into three main rain-bearing trajectory sources. The HYSPLIT model shows that the rainfall moisture comes predominately (> 85%) from the Indian Ocean (May–September), and the rest from the Western Pacific (15%) generally during October–December (Fig. 6B). Based on data from the TMD (1962–2017), Thailand is influenced by tropical storms from the South China Sea during September and October. This may contribute to the 15% of rainfall from the western Pacific to the study site.

Increased (decreased) rainfall upstream at the tropical Indian Ocean could transport ^{18}O depleted (enriched) moisture towards the western Thailand, and so contribute to a negative (positive) shift of speleothem $\delta^{18}O$. In consideration of both local, upstream amount effects, and atmospheric conditions, we interpret the speleothem $\delta^{18}O$ changes at our study site as a record of integrated changes in the rainfall amount from the ISM with minor contributions from other different moisture pathways. The lower stalagmite $\delta^{18}O$ values reflect more rainfall and vice versa. Thus, the KPC1 $\delta^{18}O$ record suggests a high variability in rainfall during 500–900 CE and 1150–1350 CE; a stable condition between 900–1150 CE, and a dry condition during 1350–1550 CE with a multi-centennial-scale dry trend from ~1350 to 1900 CE.

Furthermore, replication of speleothem $\delta^{18}O$ records from different caves in the region is important to test whether the KPC1 $\delta^{18}O$ reflects ISM rainfall variability. We compared KPC1 $\delta^{18}O$ with the speleothem $\delta^{18}O$ record from Klang cave, west coast of southern Thailand (Tan et al., 2019). On a multi-centennial scale, the two records show a good deal of consistency, e.g., frequent wet conditions during 500–900 CE and dry trends since 1350 CE (Fig. 7 a, b). The two records however slightly differ on a multi-decadal time scale, possibly due to the coarser resolution and relatively large age uncertainties of the KPC1 record. Nevertheless, the accordance of the two records supports our interpretation of the KPC1 $\delta^{18}O$ as a proxy for ISM rainfall variability, particularly on centennial time scale.

The relationship between $\delta^{13}C$ and $\delta^{18}O$ in KPC data varies through time. They are positively correlated during 500–1150 CE and 1350–1900 CE, but they show opposite trends during 1150–1350 CE. The $\delta^{13}C$ values and trace element records suggest strong local rainfall during 1150–1250 CE. In contrast, higher $\delta^{18}O$ values indicate a reduction of the integrated ISM rainfall. We also compared KPC1 $\delta^{13}C$ data with the recent speleothems $\delta^{13}C$ record from Tham Doun Mai cave, Laos (Wang et al., 2019). On a multi-centennial scale, KPC1 $\delta^{13}C$ indicates wet conditions from 500–900 CE and dry trends since 1300 CE, which are comparable with the TM-17 $\delta^{13}C$ record from Laos (Fig. 7 c, d).

These findings emphasize the importance of using multi-proxy geochemical tracers to reconstruct hydroclimate at the cave site. The $\delta^{18}O$ values probably reflect the influence of large-scale ocean-atmospheric processes rather than the total amount of precipitation at the site. Similarly, if the ISM begins earlier, more rainfall (e.g. lower $\delta^{18}O$ values) would be recorded (as opposed to an increased 'intensity'). In contrast, higher $\delta^{18}O$ values may signify more frequent monsoon breaks or a later onset of the ISM. This may explain the leads and lags between $\delta^{18}O$ and other proxies in response to past rainfall variability.

5.2 Comparison with other paleoclimatic records from Asian monsoon regions

To better understand spatial patterns of hydroclimate variability, we compared the KPC1 multi-proxy record with other paleoclimatic records (Fig. 8): (1) stalagmite $\delta^{18}O$ data from Dandak cave, India (Berkelhammer et al., 2010; Sinha et al., 2011b), (2) Palmer Drought Severity Index (PDSI) based on tree-ring data from southeast Asia

(Cook et al., 2010), (3) a multi-proxy record of Lake Pa Kho, northeastern Thailand (Chawchai et al., 2015; Yamoah et al., 2016a, 2016b), (4) sediment data from Angkor Wat and Angkor Thom reservoir in Cambodia (Day et al., 2012; Penny et al., 2019), (5) stalagmite $\delta^{13}C$ from Tham Doun Mai cave, Laos (Wang et al., 2019), (6) $\delta^{18}O$ data of ostracods from Lake Ao Tiên, Vietnam (Stevens et al., 2018), (7) grain size records from Cattle Pond on Dongdao Island, South China Sea (Yan et al., 2011), (8) stalagmite $\delta^{18}O$ data from Klang cave, southern Thailand (Tan et al., 2019), (9) a terrestrial plant leaf wax (δD_{wax}) record of marine sediments from the Makassar Strait, southwest Sulawesi (Tierney et al., 2010) and (10) a PCA of $\delta^{18}O$ stalagmite LL_{pc1} from Liang Luar cave, Flores, Indonesia (Griffiths et al., 2016).

The wetter and drier intervals (more/less rainfall) presented in Fig. 8 follow the interpretations in the original publications. Among these records, the multi-proxy record established from Lake Pa Kho, stalagmite data from Tham Doun Mai cave, Klang cave and Liang Luar cave, and the leaf wax (δD_{wax}) record from Southwest Sulawesi extend back to the last 2,000 years. Stalagmite $\delta^{18}O$ of Dandak cave in India covers the last 1,400 years. The last millennia records are from Cattle Pond and Angkor Wat reservoir, and the past 700–800 years of the Southeast Asia tree-ring data set and the Lake Ao Tiên record from Vietnam.

500–850 CE

The multi-proxy data of KPC1 suggest that on a centennial timescale, conditions alternate between wet and dry phases during 500–850 CE. This finding is consistent with the fluctuating hydroclimate conditions during 600–900 CE observed in the stalagmite $\delta^{18}O$ data from Dandak cave, India, and during 500–700 CE in Pa Kho, northeastern Thailand inferred from biomarker δD_{wax} values. Stalagmite $\delta^{13}C$ data from Tham Doun Mai cave, Laos showed more negative values associated with wetter conditions from c. 50 BCE to 750 CE. Stalagmite $\delta^{18}O$ data from Klang cave indicated an overall trend towards dry conditions for the last 2700 years, with wetter conditions from 800 BCE–900 CE. For equatorial regions, the δD_{wax} record from southwest Sulawesi showed a continuously strong rainfall from 450 to 1000 CE. Stalagmite $\delta^{18}O$ data from Liang Luar cave also suggested wetter conditions between 400–1000 CE.

850–1350 CE: Medieval Climate Anomaly (MCA)

The multi-proxy data of KPC1 indicate two-stages of hydroclimate changes in

western Thailand. During the first stage (850–1150 CE), the trace elements concentrations were low and the gray scale values were above average. However, the $\delta^{13}C$ and $\delta^{18}O$ values remained close to the average value and did not show large changes in mean hydroclimate state. During the second stage (1150–1350 CE), the $\delta^{13}C$ and $\delta^{18}O$ values show opposite trends. The low $\delta^{13}C$ values and high trace element contents suggested a strong local rainfall during 1150–1250 CE, while the high $\delta^{18}O$ values indicate a reduction of integrated rainfall along ISM trajectory. Therefore, the relatively low $\delta^{13}O$ values and high $\delta^{18}O$ values at this stage likely indicate a wet condition at the cave site but dry condition at the ocean moisture source region.

During MCA, wet conditions were inferred from stalagmite $\delta^{18}O$ at Dandak cave, India; biomarker δD_{wax} of Pa Kho, Thailand; and sediments from Angkor Wat reservoir, Cambodia. This contrasts with the southern Thailand stalagmite $\delta^{18}O$ of Klang cave, which showed dry conditions during the MCA. However, the δD_{wax} record from southwest Sulawesi also indicated drier conditions between 1000–1350 CE and a lower precipitation over Dongdao Island in the South China Sea between 1000–1400 CE. Stalagmite records from Flores, Indonesia also feature a decreased rainfall during the period of 1000–1400 CE.

1350–1550 CE: Transitional period and 1500–1900 Little Ice Age (LIA)

Centennial-long dry conditions were observed in the $\delta^{18}O$ and $\delta^{13}C$ records of KPC1 during 1350–1550 AD and in the $\delta^{18}O$ records of Dandak cave between 1300–1450 CE. Other lines of evidence came from the PDSI index record from Southeast Asia tree-ring during 1340–1370 AD and 1400–1425 CE, as well as the lake records from northeastern Thailand, Cambodia, and Vietnam during 1300–1450 CE. The driest period was also registered at Tham Douang Mai cave, Laos during 1280–1480 CE, as inferred from the $\delta^{13}C$ data. All published records in Southeast Asia showed uniformly dry conditions during the MCA–LIA transitional period.

On a multi-centennial scale, the KPC1 multi-proxy data showed oscillations around the mean but an overall trend towards dry conditions since 1350 CE. The biomarker δD_{wax} values of Pa Kho also suggested a long-term drying trend after 1350 CE. Stalagmite $\delta^{13}C$ data from Laos indicated overall drier conditions during the LIA. The stalagmite $\delta^{18}O$ of Klang cave showed dry trends after the MCA. In contrast, the $\delta^{18}O$ data of ostracods from Lake Ao Tiên, Vietnam suggested overall wetter conditions since 1500 CE. The δD_{wax} from Sulawesi indicated a stronger rainfall after 1700 CE,

509 while the stalagmites $\delta^{18}O$ records from Liang Luar cave suggested wetter conditions
510 during 1400–1900 CE.
511
512 In general, hydroclimate records from Southeast Asia support wet conditions from
513 500–800 CE (before MCA). For the last 1,200 years, the opposing hydroclimate
514 patterns between records from India and Mainland Southeast Asia in the north and the
515 equatorial region in the south have been explained by their locations relative to the
516 migration of the ITCZ (Sinha et al., 2011b; Tierney et al., 2010). A strengthened Asian
517 summer monsoon in combination with a weak Australian monsoon, would have led to
518 a shift of the tropical rain belt northward of Indonesia, leading to droughts in equatorial
519 regions during the MCA (Griffiths et al., 2016, 2009). The opposite would have been
520 the case when the Asian summer monsoon winds was weaker, and the mean position
521 of the tropical rain belt shifted over Indonesia during the LIA. Similar conclusions have
522 been drawn based on a record from the central equatorial Pacific during 1400–1900 CE
523 (Griffiths et al., 2016; Sachs et al., 2009).
524 However, the north-south migration of the ITCZ cannot explain the similar pattern
525 of the records from the western Pacific and the tropics. Yan et al. (2015) suggested a
526 latitudinal contraction in the range over which the ITCZ seasonally migrated during the
527 LIA. Denniston et al. (2016) proposed that the ITCZ/tropical rain belt expanded and
528 contracted in some regions over the last three millennia, resulting in symmetrical
529 interhemispheric changes in rainfall (i.e., drier in both the northern and southern
530 hemispheres during periods of reduced northern hemisphere temperature) rather than
531 an anti-phased response. Although, the modeled contraction of the ITCZ can explain
532 both the dry conditions at Klang cave (8^{o} N, southern Thailand) and equatorial regions
533 during the MCA, discrepancies between records from the western side of Mainland
534 Southeast Asia (such as KPC1 and Klang cave) and from the eastern side of Mainland
535 Southeast Asia (such as Vietnam) and the South China Sea are observed during the
536 LIA. The modeled contraction of the ITCZ/tropical rain belt, as proposed by Denniston
537 et al. (2016), cannot describe this east-west opposite pattern. We suggest that the ISM
538 is the dominant control on precipitation variability in the western part of Mainland
539 Southeast Asia (Myanmar and Thailand), but the PWC may have been the overriding
540 control on precipitation on the sites located closest to the EASM and WNPM (Vietnam)
541 as proposed by Yan et al. (2011) and Stevens et al. (2018).
542

543

544 **5.3. Comparison to historical records**

545 Several assumptions on the waxing and waning of the kingdoms in Southeast Asia,
546 especially "Angkor", have been formulated related to monsoon rainfall (Buckley et al.,
547 2014, 2010; Day et al., 2012; Lieberman and Buckley, 2012; Vickery, 1998). It has
548 been speculated that a decrease in rainfall and multiple extreme droughts contributed
549 to their demise (Buckley et al., 2010, 2014; Cook et al., 2010; Day et al., 2012). Here,
550 we discuss the KPC1 data together with historical records, within the context of
551 hydrological changes, during the major time events of the Late Iron Age (c. 200–600
552 CE), Pluvial Period (c. 850–1150 CE), and Elevated Hydroclimate Variability (1150–
553 1350 CE) (Fig. 5).

554 In northeastern Thailand, archeologists found a significant number of agricultural
555 tools dating back to the Late Iron Age (200–600 CE; Fig. 5), which indicate the
556 formation of complex societies (Higham et al., 2011, 2019; Higham and Higham,
557 2009). Moated settlements surrounded by multiple banks and channels are an important
558 feature of the Late Iron Age in the Mun River Valley, which is approximately 360 km
559 east from the KPC1 study site (Boyd, 2008; O'Reilly, 2008; Scott and O'Reilly, 2015).
560 It has been suggested that moats were made in response to a less reliable water supply,
561 droughts, and competition over resources (Boyd, 2008; O'Reilly, 2008; Scott and
562 O'Reilly, 2015). This represents a human response to water availability (McGrath et
563 al., 2008). For the abandonment of Late Iron Age sites (500–550 CE), Boyd (2008)
564 suggested that the social and environmental changes were a response to an increasingly
565 variable and less reliable water supply. Wohlfarth et al. (2016) have proposed that the
566 weakening of the summer monsoon stimulated a positive adaptive response involving
567 the establishment of irrigated agriculture. These historical records related to water
568 availability are comparable to the hydroclimate fluctuations inferred from multi-proxy
569 of KPC1 during 500–850 CE (Fig.5).

570 A period of ample rainfall, which seems to coincide with the MCA (900–1300 CE),
571 contributed to the early success of the 'charter states' in Mainland Southeast Asia
572 (Buckley et al., 2010, 2014; Evans et al., 2013a; Lieberman and Buckley, 2012). The
573 multi-proxy record of KPC1 suggests stable climate conditions from 850–1150 CE
574 (Fig. 5), which would support the establishment and expansion of the agrarian economy
575 that assisted the rise of the Ancient societies in Southeast Asia.

576 The KPC1 record shows a high variability in rainfall between 1150–1350 CE and

droughts in the late phase of MCA/transition to LIA (since 1350 CE), which is consistent with the new paleobotanical and stratigraphic records from sediments at Angkor Thom, Cambodia (Penny et al., 2019). This strong variability in hydroclimate conditions and long dry conditions would have executed a significant stress on human societies in the past. Together with urbanization, this may have stretched the hydrological systems to their limit. We speculate that high variability in rainfall may have played a significant role in the demise of ancient societies in Southeast Asia in the mid-15th century (Evans et al., 2013b; Lieberman and Buckley, 2012).

6. Conclusions

We present the first multi-proxy stalagmite record from western Thailand that allows a reconstruction of the hydroclimate variability over the last 1,400 years. The KPC1 multi-proxy data set reveals a high variability between wet and dry periods during 500–850 CE and 1150–1350 CE, a stable condition during 850–1150 CE, and an overall trend towards dry conditions since 1350 CE. The new KPC1 multi-proxy stalagmite data from Thailand fills a prior gap in the spatial coverage between China and Indonesia and advances our understanding of spatial patterns of Asian monsoon variability. Our study suggests that the ISM is the dominant controlling factor on precipitation variability in western Thailand. The wetness/dryness seen in India and Mainland Southeast Asia is likely due to a strengthening/weakening of the mean westerly moisture transport from the Indian Ocean. However, the PWC may have been the overriding control on precipitation at the sites located closed to the EASM and WNPM (such as the eastern sides of Mainland Southeast Asia and South China Sea). This study allows us to examine the history of civilization changes in Southeast Asia for the last 1,400 years in the context of varying hydroclimate conditions. We note that the extreme climate variability and droughts occurring at the end of ancient civilizations response to rainfall variability is consistent with the findings of previous studies based on tree-rings, lake sediments, and historical documents in Southeast Asia.

Acknowledgements

S. Chawchai wishes to express appreciation for the financial support provided by the Development and Promotion of Science Technology (DPST) Research grant 042/2558 and DAAD faculty research grant 2016. X. Wang is supported by Singapore National Research Foundation grants (2017NRF-NSFC001-047 and NRFF2011-08). D. Scholz

611 is thankful to the German Research Foundation (DFG SCHO 1274/9-1 and SCHO
612 1274/11-1). The authors also thank S. Tonongto, his family and PANDA CAMP for
613 accommodation and assistance during the field survey, M. Choowong as a mentorship
614 for SC. In addition, the authors thank officials at Ban Rai district, Uthai Thani province
615 for their help and hospitality. We also thank S. Mischel for his help with TERMITE
616 and A. Budsky for cutting the sample for LA-ICP-MS analysis, W. Suwansukho and P.
617 Rattanasrimongkol for polishing the samples and discussion, and the Research Clinic
618 Unit, Office of Research Affairs at Chulalongkorn University for assistance during
619 manuscript preparation.

620

621 **Figure captions**

622 **Fig. 1(A)**. Annual total precipitation (mm, GPCP). **(B)** Locations of Khao Prae cave
623 (white star), western Thailand. **(C)** Mean monthly rainfall and temperature (1962–2017
624 AD) for Uthai Thani province, which is situated 50 km NE to Khao Prae cave. GPCP
625 Precipitation data are provided by the NOAA/OAR/ESRL PSD, Boulder, Colorado,
626 USA, from their Web site at https://www.esrl.noaa.gov/psd/

627

628 **Fig. 2 (A)** Two-dimensional images of the KPC1 sample from a CT scan in grayscale.
629 Lower densities are indicated by a darker grayscale color and vice versa. **(B)** Halved
630 sections of stalagmite KPC1. Red squares show the locations for XRD analysis. Red
631 arrows show possible location of a hiatus.

632

633 **Fig. 3 (A)** Halved sections of the stalagmite with locations for dating and the results
634 from the **(B)** StalAge and **(C)** BACON age models. The blue shapes show the dates
635 with two standard deviations, the green line indicates the likely age model, and the red
636 lines show the 95% confidence ranges of the age models. See Table 1 for U-Th ages.

637

638 **Fig. 4 (A)** Transect sections of stalagmite KPC1, where the red line shows transect
639 drilled for trace element analysis and blue dotted line for $\delta^{13}C$ and $\delta^{18}O$ analysis **(B)**
640 Gray scale values and elemental profiles of **(C)** Fe, **(D)** Mn, **(E)** Zn, and **(F)** Cu.

641

642 **Fig. 5** Time series of **(A)** elemental profile of Fe, **(B)** gray scale values, **(C)** $\delta^{13}C$ values,
643 and **(D)** $\delta^{18}O$ values. Gray color bars represent intervals of higher trace element

644 compositions. Blue color reflects wet conditions/strong rainfall and brown color
645 represent dry conditions at the cave site.
646
647 **Fig. 6 (A)** Monthly mean $\delta^{18}O$ values and monthly mean amount of rainfall from 2016
648 to 2017 in Uthai Thani province **(B)** NOAA's Hybrid Single Particle Langarian
649 Integrated Trajectory (HYSPLIT4) model with the NCAR/NCEP Reanalysis 2.5 deg
650 gridded data set. HYSPLIT4 was used to analyze daily 6-day back trajectories from
651 the site at 15°05' N, 99°25' E from 2000–2009. The rain-bearing trajectories (> 8.5
652 mm/day) were selected based on rainfall amounts derived from ERA-Interim data
653 downloaded from the ECMWF public datasets and clustered into three main rain-
654 bearing trajectory sources.
655
656 **Fig. 7** Comparison of the KPC1 record with other speleothem records from
657 Mainland Southeast Asia (a) Stalagmite TM-17 $\delta^{13}C$ from Tham Doun Mai cave, Laos
658 (Wang et al., 2019), (b) Stalagmite KPC 1 $\delta^{13}C$ and (c) KPC 1 $\delta^{18}O$ (this study), and
659 (d) Stalagmite TK from Klang cave, southern Thailand (Tan et al., 2019). Blue color
660 bar reflects wet conditions/strong rainfall and brown color bar represents dry
661 conditions.
662
663 **Fig. 8** Location of Asian monsoon paleo-records for the last 2000 years. Spatial and
664 temporal variability of the paleoclimatic reconstructed from: (1) stalagmite $\delta^{18}O$ data
665 from Dandak cave, India (Berkelhammer et al., 2010; Sinha et al., 2011b), (2) Palmer
666 Drought Severity Index (PDSI) based on tree-ring data from southeast Asia (Cook et
667 al., 2010), (3) a multi-proxy record of Lake Pa Kho, northeastern Thailand (Chawchai
668 et al., 2015; Yamoah et al., 2016a, 2016b), (4) sediment data from Angkor Wat and
669 Angkor Thom reservoir in Cambodia (Day et al., 2012; Penny et al., 2019), (5)
670 stalagmite $\delta^{13}C$ from Tham Doun Mai cave, Laos (Wang et al., 2019), (6) $\delta^{18}O$ data of
671 ostracods from Lake Ao Tiên, Vietnam (Stevens et al., 2018), (7) grain size records
672 from Cattle Pond on Dongdao Island, South China Sea (Yan et al., 2011), (8) stalagmite
673 $\delta^{18}O$ data from Klang cave, southern Thailand (Tan et al., 2019), (9) a terrestrial plant
674 leaf wax (δD_{wax}) record of marine sediments from the Makassar Strait, southwest
675 Sulawesi (Tierney et al., 2010), and (10) a PCA of $\delta^{18}O$ stalagmite LL_{pc1} from Liang
676 Luar cave, Flores, Indonesia (Griffiths et al., 2016).

677
678
679
680 **Table captions**
681
682 **Table 1** U and Th isotopic compositions (^{238}U, ^{234}U, ^{232}Th, and ^{230}Th) and $^{230}Th/U$ ages
683 for subsamples of stalagmites KPC1. U decay constants: $\lambda_{238} = 1.55125 \times 10^{-10}$ (Jaffey
684 et al., 1971) and $\lambda_{234} = 2.82206 \times 10^{-6}$ (Cheng et al., 2013). Th decay constant: $\lambda_{230} =$
685 9.1705×10^{-6} (Cheng et al., 2013). *$\delta^{234}U = ([^{234}U/^{238}U]_{activity} - 1) \times 1000$. **$\delta^{234}U_{initial}$
686 was calculated based on ^{230}Th age (T), i.e., $\delta^{234}U_{initial} = \delta^{234}U_{measured} \times e^{\lambda 234 \times T}$. Corrected
687 ^{230}Th ages assume the initial $^{230}Th/^{232}Th$ atomic ratio of $2.73 \pm 0.21 \times 10^{-6}$. ***B.P.
688 stands for "Before Present" where the "Present" is defined as the year 1950 CE.
689
690
691 **References**

692 Bajo, P., Hellstrom, J., Frisia, S., Drysdale, R., Black, J., Woodhead, J., Borsato, A.,
693 Zanchetta, G., Wallace, M.W., Regattieri, E., Haese, R., 2016. "Cryptic"
694 diagenesis and its implications for speleothem geochronologies. Quat. Sci.
695 Rev. 148, 17–28. https://doi.org/10.1016/j.quascirev.2016.06.020
696 Baker, A., Ito, E., Smart, P.L., McEwan, R.F., 1997. Elevated and variable values of
697 13C in speleothems in a British cave system. Chem. Geol. 136, 263–270.
698 https://doi.org/10.1016/S0009-2541(96)00129-5
699 Baker, A., Smith, C., Jex, C., Fairchild, I.J., Genty, D., Fuller, L., 2008. Annually
700 laminated speleotherms : a review. Int. J. Speleol. 37, 193–206.
701 Beck, J.W., Zhou, W., Li, C., Wu, Z., White, L., Xian, F., Kong, X., An, Z., 2018. A
702 550,000-year record of East Asian monsoon rainfall from 10Be in loess.
703 Science 360, 877–881. https://doi.org/10.1126/science.aam5825
704 Berkelhammer, M., Sinha, A., Mudelsee, M., Cheng, H., Edwards, R.L., Cannariato,
705 K., 2010. Persistent multidecadal power of the Indian Summer Monsoon.
706 Earth Planet. Sci. Lett. 290, 166–172.
707 https://doi.org/10.1016/j.epsl.2009.12.017
708 Blaauw, M., Christen, J.A., 2011. Flexible paleoclimate age-depth models using an
709 autoregressive gamma process. Bayesian Anal. 6, 457–474.
710 https://doi.org/10.1214/11-BA618
711 Blaser, P., Zimmermann, S., Luster, J., Shotyk, W., 2000. Critical examination of
712 trace element enrichments and depletions in soils: As, Cr, Cu, Ni, Pb, and Zn
713 in Swiss forest soils. Sci. Total Environ. 249, 257–280.
714 https://doi.org/10.1016/S0048-9697(99)00522-7
715 Borsato, A., Frisia, S., Fairchild, I.J., Somogyi, A., Susini, J., 2007. Trace element
716 distribution in annual stalagmite laminae mapped by micrometer-resolution X-
717 ray fluorescence: Implications for incorporation of environmentally significant
718 species. Geochim. Cosmochim. Acta 71, 1494–1512. https://doi.org/doi: DOI:
719 10.1016/j.gca.2006.12.016

720 Boyd, W.E., 2008. Social change in late Holocene mainland SE Asia: A response to
721 gradual climate change or a critical climatic event? Quat. Int., Environmental
722 Variability and Human Adaptation in the Pacific Rim and the Sustainability of
723 the Islands 184, 11–23. https://doi.org/10.1016/j.quaint.2007.09.017
724 Breitenbach, S.F.M., Adkins, J.F., Meyer, H., Marwan, N., Kumar, K.K., Haug, G.H.,
725 2010. Strong influence of water vapor source dynamics on stable isotopes in
726 precipitation observed in Southern Meghalaya, NE India. Earth Planet. Sci.
727 Lett. 292, 212–220. https://doi.org/10.1016/j.epsl.2010.01.038
728 Breitenbach, S.F.M., Lechleitner, F.A., Meyer, H., Diengdoh, G., Mattey, D.,
729 Marwan, N., 2015. Cave ventilation and rainfall signals in dripwater in a
730 monsoonal setting – a monitoring study from NE India. Chem. Geol. 402,
731 111–124. https://doi.org/10.1016/j.chemgeo.2015.03.011
732 Buckley, B.M., Anchukaitis, K.J., Penny, D., Fletcher, R., Cook, E.R., Sano, M.,
733 Nam, L.C., Wichienkeeo, A., Minh, T.T., Hong, T.M., 2010. Climate as a
734 contributing factor in the demise of Angkor, Cambodia. Proc. Natl. Acad. Sci.
735 107, 6748–6752. https://doi.org/10.1073/pnas.0910827107
736 Buckley, B.M., Fletcher, R., Wang, S.-Y.S., Zottoli, B., Pottier, C., 2014. Monsoon
737 extremes and society over the past millennium on mainland Southeast Asia.
738 Quat. Sci. Rev. 95, 1–19. https://doi.org/10.1016/j.quascirev.2014.04.022
739 Cai, B., Pumijumnong, N., Tan, M., Muangsong, C., Kong, X., Jiang, X., Nan, S.,
740 2010. Effects of intraseasonal variation of summer monsoon rainfall on stable
741 isotope and growth rate of a stalagmite from northwestern Thailand. J.
742 Geophys. Res. Atmospheres 115. https://doi.org/10.1029/2009JD013378
743 Caley, T., Roche, D.M., Renssen, H., 2014. Orbital Asian summer monsoon dynamics
744 revealed using an isotope-enabled global climate model. Nat. Commun. 5,
745 5371. https://doi.org/10.1038/ncomms6371
746 Chawchai, S., Chabangborn, A., Fritz, S., Väliranta, M., Mörth, C.-M., Blaauw, M.,
747 Reimer, P.J., Krusic, P.J., Löwemark, L., Wohlfarth, B., 2015. Hydroclimatic
748 shifts in northeast Thailand during the last two millennia – the record of Lake
749 Pa Kho. Quat. Sci. Rev. 111, 62–71.
750 https://doi.org/10.1016/j.quascirev.2015.01.007
751 Chawchai, S., Liu Guangxin, Bissen Raphael, Jankham Kampanart, Paisonjumlongsri
752 Warisa, Kanjanapayont Pitsanupong, Chutakositkanon Vichai, Choowong
753 Montri, Pailoplee Santi, Wang Xianfeng, 2018. Stalagmites from western
754 Thailand: preliminary investigations and challenges for palaeoenvironmental
755 research. Boreas 47, 367–376. https://doi.org/10.1111/bor.12299
756 Cheng, H., Edwards, R.L., Sinha, A., Spötl, C., Yi, L., Chen, S., Kelly, M., Kathayat,
757 G., Wang, X., Li, X., Kong, X., Wang, Y., Ning, Y., Zhang, H., 2016. The
758 Asian monsoon over the past 640,000 years and ice age terminations. Nature
759 534, 640–646. https://doi.org/10.1038/nature18591
760 Chiang, H.-W., Lu, Y., Wang, X., Lin, K., Liu, X., 2019. Optimizing MC-ICP-MS
761 with SEM protocols for determination of U and Th isotope ratios and 230Th
762 ages in carbonates. Quat. Geochronol. 50, 75–90.
763 https://doi.org/10.1016/j.quageo.2018.10.003
764 Chiang, J.C.H., Fung, I.Y., Wu, C.-H., Cai, Y., Edman, J.P., Liu, Y., Day, J.A.,
765 Bhattacharya, T., Mondal, Y., Labrousse, C.A., 2015. Role of seasonal
766 transitions and westerly jets in East Asian paleoclimate. Quat. Sci. Rev. 108,
767 111–129. https://doi.org/10.1016/j.quascirev.2014.11.009
768 Clemens, S.C., Prell, W.L., Sun, Y., 2010. Orbital-scale timing and mechanisms
769 driving Late Pleistocene Indo-Asian summer monsoons: Reinterpreting cave

speleothem δ18O. Paleoceanography 25. https://doi.org/10.1029/2010PA001926

Conroy, J.L., Overpeck, J.T., 2011. Regionalization of Present-Day Precipitation in the Greater Monsoon Region of Asia *. J. Clim. 24, 4073–4095. https://doi.org/10.1175/2011JCLI4033.1

Cook, E.R., Anchukaitis, K.J., Buckley, B.M., D'Arrigo, R.D., Jacoby, G.C., Wright, W.E., 2010. Asian Monsoon Failure and Megadrought During the Last Millennium. Science 328, 486–489. https://doi.org/10.1126/science.1185188

Dansgaard, W., 1964. Stable isotopes in precipitation. Tellus XVI, 436 – 468.

D'Arrigo, R., Ummenhofer, C.C., 2015. The climate of Myanmar: evidence for effects of the Pacific Decadal Oscillation. Int. J. Climatol. 35, 634–640. https://doi.org/10.1002/joc.3995

Day, M.B., Hodell, D.A., Brenner, M., Chapman, H.J., Curtis, J.H., Kenney, W.F., Kolata, A.L., Peterson, L.C., 2012. Paleoenvironmental history of the West Baray, Angkor (Cambodia). Proc. Natl. Acad. Sci. 109, 1046–1051. https://doi.org/10.1073/pnas.1111282109

Dayem, K.E., Molnar, P., Battisti, D.S., Roe, G.H., 2010. Lessons learned from oxygen isotopes in modern precipitation applied to interpretation of speleothem records of paleoclimate from eastern Asia. Earth Planet. Sci. Lett. 295, 219–230. https://doi.org/doi: DOI: 10.1016/j.epsl.2010.04.003

Deininger, M., Fohlmeister, J., Scholz, D., Mangini, A., 2012. Isotope disequilibrium effects: The influence of evaporation and ventilation effects on the carbon and oxygen isotope composition of speleothems – A model approach. Geochim. Cosmochim. Acta 96, 57–79. https://doi.org/10.1016/j.gca.2012.08.013

Denniston, R.F., González, L.A., Asmerom, Y., Sharma, R.H., Reagan, M.K., 2000. Speleothem Evidence for Changes in Indian Summer Monsoon Precipitation over the Last ~2300 Years. Quat. Res. 53, 196–202. https://doi.org/10.1006/qres.1999.2111

Denniston, R.F., Ummenhofer, C.C., Wanamaker, A.D., Lachniet, M.S., Villarini, G., Asmerom, Y., Polyak, V.J., Passaro, K.J., Cugley, J., Woods, D., Humphreys, W.F., 2016. Expansion and Contraction of the Indo-Pacific Tropical Rain Belt over the Last Three Millennia. Sci. Rep. 6, 34485. https://doi.org/10.1038/srep34485

Department of Mineral Resources (DMR), 2009. Geological Map of Changwat Udon Thani, Scale 1:250,000.

Dettman, D.L., Lohmann, K.C., 1995. Microsampling Carbonates for Stable Isotope and Minor Element Analysis: Physical Separation of Samples on a 20 Micrometer Scale: RESEARCH METHOD PAPER. J. Sediment. Res. 65.

Ding, R., Ha, K.-J., Li, J., 2010. Interdecadal shift in the relationship between the East Asian summer monsoon and the tropical Indian Ocean. Clim. Dyn. 34, 1059–1071. https://doi.org/10.1007/s00382-009-0555-2

Dykoski, C.A., Edwards, R.L., Cheng, H., Yuan, D., Cai, Y., Zhang, M., Lin, Y., Qing, J., An, Z., Revenaugh, J., 2005. A high-resolution, absolute-dated Holocene and deglacial Asian monsoon record from Dongge Cave, China. Earth Planet. Sci. Lett. 233, 71–86. https://doi.org/10.1016/j.epsl.2005.01.036

Edwards, R.L., Chen, J.H., Wasserburg, G.J., 1986. 238U-234U-230Th-232Th systematics and the precise measurement of time over the past 500,000 years. Earth Planet. Sci. Lett. 81, 175–192.

Eroglu, D., McRobie, F.H., Ozken, I., Stemler, T., Wyrwoll, K.-H., Breitenbach, S.F.M., Marwan, N., Kurths, J., 2016. See–saw relationship of the Holocene

East Asian–Australian summer monsoon. Nat. Commun. 7, 12929. https://doi.org/10.1038/ncomms12929

Evans, D.H., Fletcher, R.J., Pottier, C., Chevance, J.-B., Soutif, D., Tan, B.S., Im, S., Ea, D., Tin, T., Kim, S., Cromarty, C., Greef, S.D., Hanus, K., Bâty, P., Kuszinger, R., Shimoda, I., Boornazian, G., 2013a. Uncovering archaeological landscapes at Angkor using lidar. Proc. Natl. Acad. Sci. 110, 12595–12600. https://doi.org/10.1073/pnas.1306539110

Evans, D.H., Fletcher, R.J., Pottier, C., Chevance, J.-B., Soutif, D., Tan, B.S., Im, S., Ea, D., Tin, T., Kim, S., Cromarty, C., Greef, S.D., Hanus, K., Bâty, P., Kuszinger, R., Shimoda, I., Boornazian, G., 2013b. Uncovering archaeological landscapes at Angkor using lidar. Proc. Natl. Acad. Sci. https://doi.org/10.1073/pnas.1306539110

Fairchild, I.J., Smith, C.L., Baker, A., Fuller, L., Spötl, C., Mattey, D., McDermott, F., E.i.m.f., 2006. Modification and preservation of environmental signals in speleothems. Earth-Sci. Rev., ISOtopes in PALaeoenvironmental reconstruction (ISOPAL) 75, 105–153. https://doi.org/10.1016/j.earscirev.2005.08.003

Fairchild, I.J., Treble, P.C., 2009a. Trace elements in speleothems as recorders of environmental change. Quat. Sci. Rev. 28, 449–468. https://doi.org/10.1016/j.quascirev.2008.11.007

Fairchild, I.J., Treble, P.C., 2009b. Trace elements in speleothems as recorders of environmental change. Quat. Sci. Rev. 28, 449–468. https://doi.org/10.1016/j.quascirev.2008.11.007

Fohlmeister, J., Scholz, D., Kromer, B., Mangini, A., 2011. Modelling carbon isotopes of carbonates in cave drip water. Geochim. Cosmochim. Acta 75, 5219–5228. https://doi.org/10.1016/j.gca.2011.06.023

Griffiths, M.L., Drysdale, R.N., Gagan, M.K., Zhao, J. -x, Ayliffe, L.K., Hellstrom, J.C., Hantoro, W.S., Frisia, S., Feng, Y. -x, Cartwright, I., Pierre, E.S., Fischer, M.J., Suwargadi, B.W., 2009. Increasing Australian–Indonesian monsoon rainfall linked to early Holocene sea-level rise. Nat. Geosci. 2, 636–639. https://doi.org/10.1038/ngeo605

Griffiths, M.L., Kimbrough, A.K., Gagan, M.K., Drysdale, R.N., Cole, J.E., Johnson, K.R., Zhao, J.-X., Cook, B.I., Hellstrom, J.C., Hantoro, W.S., 2016. Western Pacific hydroclimate linked to global climate variability over the past two millennia. Nat. Commun. 7, 11719. https://doi.org/10.1038/ncomms11719

Hartland, A., Zitoun, R., 2018. Transition metal availability to speleothems controlled by organic binding ligands 8, 22–25. https://doi.org/10.7185/geochemlet.1824

Haug, G.H., Hughen, K.A., Sigman, D.M., Peterson, L.C., Röhl, U., 2001. Southward Migration of the Intertropical Convergence Zone Through the Holocene. Science 293, 1304–1308. https://doi.org/10.1126/science.1059725

Hellstrom, J., 2006. U–Th dating of speleothems with high initial 230Th using stratigraphical constraint. Quat. Geochronol. 1, 289–295. https://doi.org/10.1016/j.quageo.2007.01.004

Hendy, C.H., 1971. The isotopic geochemistry of speleothems--I. The calculation of the effects of different modes of formation on the isotopic composition of speleothems and their applicability as palaeoclimatic indicators. Geochim. Cosmochim. Acta 35, 801–824. https://doi.org/doi: DOI: 10.1016/0016-7037(71)90127-X

868 Higham, C., Higham, T., 2009. A new chronological framework for prehistoric
869 Southeast Asia, based on a Bayesian model from Ban Non Wat. Antiquity 83,
870 125–144.
871 Higham, C., Higham, T., Ciarla, R., Douka, K., Kijngam, A., Rispoli, F., 2011. The
872 Origins of the Bronze Age of Southeast Asia. J. World Prehistory 24, 227–
873 274. https://doi.org/10.1007/s10963-011-9054-6
874 Higham, C.F.W., Manly, B.F.J., Thosarat, R., Buckley, H.R., Chang, N., Halcrow,
875 S.E., Ward, S., O'Reilly, D.J.W., Shewan, L.G., Domett, K., 2019.
876 Environmental and Social Change in Northeast Thailand during the Iron Age.
877 Camb. Archaeol. J. 1–21. https://doi.org/10.1017/S0959774319000192
878 Jochum, K.P., Nohl, U., Herwig, K., Lammel, E., Stoll, B., Hofmann, A.W., 2005.
879 GeoReM: A New Geochemical Database for Reference Materials and Isotopic
880 Standards. Geostand. Geoanalytical Res. 29, 333–338.
881 https://doi.org/10.1111/j.1751-908X.2005.tb00904.x
882 Jochum, K.P., Scholz, D., Stoll, B., Weis, U., Wilson, S.A., Yang, Q., Schwalb, A.,
883 Börner, N., Jacob, D.E., Andreae, M.O., 2012. Accurate trace element analysis
884 of speleothems and biogenic calcium carbonates by LA-ICP-MS. Chem. Geol.
885 318–319, 31–44. https://doi.org/10.1016/j.chemgeo.2012.05.009
886 Jochum, K.P., Weis, U., Stoll, B., Kuzmin, D., Yang, Q., Raczek, I., Jacob, D.E.,
887 Stracke, A., Birbaum, K., Frick, D.A., Günther, D., Enzweiler, J., 2011.
888 Determination of Reference Values for NIST SRM 610–617 Glasses
889 Following ISO Guidelines. Geostand. Geoanalytical Res. 35, 397–429.
890 https://doi.org/10.1111/j.1751-908X.2011.00120.x
891 Johnson, K.R., Ingram, B.L., 2004. Spatial and temporal variability in the stable
892 isotope systematics of modern precipitation in China: implications for
893 paleoclimate reconstructions. Earth Planet. Sci. Lett. 220, 365–377.
894 https://doi.org/10.1016/S0012-821X(04)00036-6
895 Kathayat, G., Cheng, H., Sinha, A., Yi, L., Li, X., Zhang, H., Li, H., Ning, Y.,
896 Edwards, R.L., 2017. The Indian monsoon variability and civilization changes
897 in the Indian subcontinent. Sci. Adv. 3, e1701296.
898 https://doi.org/10.1126/sciadv.1701296
899 Krause, C.E., Gagan, M.K., Dunbar, G.B., Hantoro, W.S., Hellstrom, J.C., Cheng, H.,
900 Edwards, R.L., Suwargadi, B.W., Abram, N.J., Rifai, H., 2019. Spatio-
901 temporal evolution of Australasian monsoon hydroclimate over the last 40,000
902 years. Earth Planet. Sci. Lett. 513, 103–112.
903 https://doi.org/10.1016/j.epsl.2019.01.045
904 Li, D., Tan, L., Cai, Y., Jiang, X., Ma, L., Cheng, H., Edwards, R.L., Zhang, H., Gao,
905 Y., An, Z., 2019. Is Chinese stalagmite δ18O solely controlled by the Indian
906 summer monsoon? Clim. Dyn. https://doi.org/10.1007/s00382-019-04671-x
907 Lieberman, V., Buckley, B., 2012. The Impact of Climate on Southeast Asia, circa
908 950–1820: New Findings. Mod. Asian Stud. 1–48.
909 https://doi.org/10.1017/S0026749X12000091
910 Liu, D., Wang, Y., Cheng, H., Edwards, R.L., Kong, X., Li, T.-Y., 2016. Strong
911 coupling of centennial-scale changes of Asian monsoon and soil processes
912 derived from stalagmite δ18O and δ13C records, southern China. Quat. Res.
913 85, 333–346. https://doi.org/10.1016/j.yqres.2016.02.008
914 Liu, J., Chen, J., Zhang, X., Li, Y., Rao, Z., Chen, F., 2015. Holocene East Asian
915 summer monsoon records in northern China and their inconsistency with
916 Chinese stalagmite δ18O records. Earth-Sci. Rev. 148, 194–208.
917 https://doi.org/10.1016/j.earscirev.2015.06.004

Liu, Z., Wen, X., Brady, E.C., Otto-Bliesner, B., Yu, G., Lu, H., Cheng, H., Wang, Y., Zheng, W., Ding, Y., Edwards, R.L., Cheng, J., Liu, W., Yang, H., 2014. Chinese cave records and the East Asia Summer Monsoon. Quat. Sci. Rev. 83, 115–128. https://doi.org/10.1016/j.quascirev.2013.10.021

Mann, M.E., Jones, P.D., 2003. Global surface temperatures over the past two millennia. Geophys. Res. Lett. 30, 1820. https://doi.org/10.1029/2003GL017814

McDermott, F., 2004. Palaeo-climate reconstruction from stable isotope variations in speleothems: a review. Quat. Sci. Rev., Isotopes in Quaternary Paleoenvironmental reconstruction 23, 901–918. https://doi.org/10.1016/j.quascirev.2003.06.021

McGrath, R.J., Boyd, W.E., Bush, R.T., 2008. The paleohydrological context of the Iron Age floodplain sites of the Mun River Valley, Northeast Thailand1. Geoarchaeology 23, 151–172. https://doi.org/10.1002/gea.20210

Mickler, P.J., Ketcham, R.A., Colbert, M.W., Banner, J.L., 2004. Application of high-resolution X-ray computed tomography in determining the suitability of speleothems for use in paleoclimatic, paleohydrologic reconstructions. J. Cave Karst Stud. 66, 3–8.

Mischel, S.A., Mertz-Kraus, R., Jochum, K.P., Scholz, D., 2017. TERMITE: An R script for fast reduction of laser ablation inductively coupled plasma mass spectrometry data and its application to trace element measurements. Rapid Commun. Mass Spectrom. 31, 1079–1087. https://doi.org/10.1002/rcm.7895

Moberg, A., Sonechkin, D.M., Holmgren, K., Datsenko, N.M., Karlén, W., 2005. Highly variable Northern Hemisphere temperatures reconstructed from low- and high-resolution proxy data. Nature 433, 613–617. https://doi.org/10.1038/nature03265

Muangsong, C., Cai, B., Pumijumnong, N., Hu, C., Cheng, H., 2014. An annually laminated stalagmite record of the changes in Thailand monsoon rainfall over the past 387 years and its relationship to IOD and ENSO. Quat. Int., Quaternary of East Asia and the Western Pacific: Part 2 349, 90–97. https://doi.org/10.1016/j.quaint.2014.08.037

O'Neil, J.R., Clayton, R.N., Mayeda, T.K., 1969. Oxygen Isotope Fractionation in Divalent Metal Carbonates. J. Chem. Phys. 51, 5547–5558. https://doi.org/10.1063/1.1671982

O'Reilly, D.J.W., 2008. Multivallate sites and socio-economic change: Thailand and Britain in their Iron Ages. Antiquity 82, 377–389. https://doi.org/10.1017/S0003598X00096873

Partin, J.W., Cobb, K.M., Adkins, J.F., Clark, B., Fernandez, D.P., 2007. Millennial-scale trends in west Pacific warm pool hydrology since the Last Glacial Maximum. Nature 449, 452–455. https://doi.org/10.1038/nature06164

Pausata, F.S.R., Battisti, D.S., Nisancioglu, K.H., Bitz, C.M., 2011a. Chinese stalagmite $\delta^{18}O$ controlled by changes in the Indian monsoon during a simulated Heinrich event. Nat. Geosci. 4, 474–480. https://doi.org/10.1038/ngeo1169

Pausata, F.S.R., Battisti, D.S., Nisancioglu, K.H., Bitz, C.M., 2011b. Chinese stalagmite δ18O controlled by changes in the Indian monsoon during a simulated Heinrich event. Nat. Geosci. 4, 474–480. https://doi.org/10.1038/ngeo1169

Penny, D., Hall, T., Evans, D., Polkinghorne, M., 2019. Geoarchaeological evidence from Angkor, Cambodia, reveals a gradual decline rather than a catastrophic

968 15th-century collapse. Proc. Natl. Acad. Sci. 201821460.
969 https://doi.org/10.1073/pnas.1821460116
970 Raghavan, S.V., Liu, J., Nguyen, N.S., Vu, M.T., Liong, S.-Y., 2018. Assessment of
971 CMIP5 historical simulations of rainfall over Southeast Asia. Theor. Appl.
972 Climatol. 132, 989–1002. https://doi.org/10.1007/s00704-017-2111-z
973 Räsänen, T.A., Lindgren, V., Guillaume, J.H.A., Buckley, B.M., Kummu, M., 2016.
974 On the spatial and temporal variability of ENSO precipitation and drought
975 teleconnection in mainland Southeast Asia. Clim Past 12, 1889–1905.
976 https://doi.org/10.5194/cp-12-1889-2016
977 Richards, D.A., Dorale, J.A., 2003. Uranium-series Chronology and Environmental
978 Applications of Speleothems. Rev. Mineral. Geochem. 52, 407–460.
979 https://doi.org/10.2113/0520407
980 Ruan, J., Zhang, H., Cai, Z., Yang, X., Yin, J., 2019. Regional controls on daily to
981 interannual variations of precipitation isotope ratios in Southeast China:
982 Implications for paleomonsoon reconstruction. Earth Planet. Sci. Lett. 527,
983 115794. https://doi.org/10.1016/j.epsl.2019.115794
984 Sachs, J.P., Sachse, D., Smittenberg, R.H., Zhang, Z., Battisti, D.S., Golubic, S.,
985 2009. Southward movement of the Pacific intertropical convergence zone
986 AD 1400–1850. Nat. Geosci. 2, 519–525. https://doi.org/10.1038/ngeo554
987 Scholz, D., Hoffmann, D.L., 2011. StalAge – An algorithm designed for construction
988 of speleothem age models. Quat. Geochronol. 6, 369–382.
989 https://doi.org/10.1016/j.quageo.2011.02.002
990 Scott, G., O'Reilly, D., 2015. Rainfall and circular moated sites in north-east
991 Thailand. Antiquity 89, 1125–1138. https://doi.org/10.15184/aqy.2015.130
992 Shen, C.-C., Wu, C.-C., Cheng, H., Lawrence Edwards, R., Hsieh, Y.-T., Gallet, S.,
993 Chang, C.-C., Li, T.-Y., Lam, D.D., Kano, A., Hori, M., Spötl, C., 2012. High-
994 precision and high-resolution carbonate 230Th dating by MC-ICP-MS with
995 SEM protocols. Geochim. Cosmochim. Acta 99, 71–86.
996 https://doi.org/10.1016/j.gca.2012.09.018
997 Shopov, Y.Y., Ford, D.C., Schwarcz, H.P., 1994. Luminescent microbanding in
998 speleothems: High-resolution chronology and paleoclimate. Geology 22, 407–
999 410. https://doi.org/10.1130/0091-7613(1994)022<0407:LMISHR>2.3.CO;2
1000 Singhrattna, N., Rajagopalan, B., Kumar, K.K., Clark, M., 2005. Interannual and
1001 Interdecadal Variability of Thailand Summer Monsoon Season. J. Clim. 18,
1002 1697–1708. https://doi.org/10.1175/JCLI3364.1
1003 Sinha, A., Berkelhammer, M., Stott, L., Mudelsee, M., Cheng, H., Biswas, J., 2011a.
1004 The leading mode of Indian Summer Monsoon precipitation variability during
1005 the last millennium. Geophys. Res. Lett. 38.
1006 https://doi.org/10.1029/2011GL047713
1007 Sinha, A., Cannariato, K.G., Stott, L.D., Cheng, H., Edwards, R.L., Yadava, M.G.,
1008 Ramesh, R., Singh, I.B., 2007. A 900-year (600 to 1500 A.D.) record of the
1009 Indian summer monsoon precipitation from the core monsoon zone of India.
1010 Geophys. Res. Lett. 34, L16707. https://doi.org/10.1029/2007GL030431
1011 Sinha, A., Stott, L., Berkelhammer, M., Cheng, H., Edwards, R.L., Buckley, B.,
1012 Aldenderfer, M., Mudelsee, M., 2011b. A global context for megadroughts in
1013 monsoon Asia during the past millennium. Quat. Sci. Rev. 30, 47–62.
1014 https://doi.org/10.1016/j.quascirev.2010.10.005
1015 Stevens, L.R., Buckley, B.M., Kim, S., Hill, P., Doiron, K., 2018. Increased effective
1016 moisture in northern Vietnam during the Little Ice Age. Palaeogeogr.

1017 Palaeoclimatol. Palaeoecol. 511, 449–461.
1018 https://doi.org/10.1016/j.palaeo.2018.09.011
1019 Tan, L., Cai, Y., An, Z., Cheng, H., Shen, C.-C., Breitenbach, S.F.M., Gao, Y.,
1020 Edwards, R.L., Zhang, H., Du, Y., 2015. A Chinese cave links climate change,
1021 social impacts and human adaptation over the last 500 years. Sci. Rep. 5, 1–
1022 10. https://doi.org/10.1038/srep12284
1023 Tan, L., Cai, Y., An, Z., Cheng, H., Shen, C.-C., Gao, Y., Edwards, R.L., 2017.
1024 Decreasing monsoon precipitation in southwest China during the last 240
1025 years associated with the warming of tropical ocean. Clim. Dyn. 48, 1769–
1026 1778. https://doi.org/10.1007/s00382-016-3171-y
1027 Tan, L., Cai, Y., An, Z., Edwards, R.L., Cheng, H., Shen, C.-C., Zhang, H., 2011.
1028 Centennial- to decadal-scale monsoon precipitation variability in the semi-
1029 humid region, northern China during the last 1860 years: Records from
1030 stalagmites in Huangye Cave. The Holocene 21, 287–296.
1031 https://doi.org/10.1177/0959683610378880
1032 Tan, L., Cai, Y., Cheng, H., An, Z., Edwards, R.L., 2009. Summer monsoon
1033 precipitation variations in central China over the past 750years derived from a
1034 high-resolution absolute-dated stalagmite. Palaeogeogr. Palaeoclimatol.
1035 Palaeoecol. 280, 432–439. https://doi.org/10.1016/j.palaeo.2009.06.030
1036 Tan, L., Shen, C.-C., Löwemark, L., Chawchai, S., Edwards, R.L., Cai, Y.,
1037 Breitenbach, S.F.M., Cheng, H., Chou, Y.-C., Duerrast, H., Partin, J.W., Cai,
1038 W., Chabangborn, A., Gao, Y., Kwiecien, O., Wu, C.-C., Shi, Z., Hsu, H.-H.,
1039 Wohlfarth, B., 2019. Rainfall variations in central Indo-Pacific over the past
1040 2,700 y. Proc. Natl. Acad. Sci. 201903167.
1041 https://doi.org/10.1073/pnas.1903167116
1042 Tan, M., 2016. Circulation background of climate patterns in the past millennium:
1043 Uncertainty analysis and re-reconstruction of ENSO-like state. Sci. China
1044 Earth Sci. 59, 1225–1241. https://doi.org/10.1007/s11430-015-5256-6
1045 Tan, M., Baker, A., Genty, D., Smith, C., Esper, J., Cai, B., 2006. Applications of
1046 stalagmite laminae to paleoclimate reconstructions: Comparison with
1047 dendrochronology/climatology. Quat. Sci. Rev. 25, 2103–2117.
1048 https://doi.org/10.1016/j.quascirev.2006.01.034
1049 Thirumalai, K., DiNezio, P.N., Okumura, Y., Deser, C., 2017. Extreme temperatures
1050 in Southeast Asia caused by El Niño and worsened by global warming. Nat.
1051 Commun. 8, 15531. https://doi.org/10.1038/ncomms15531
1052 Tierney, J.E., Oppo, D.W., Rosenthal, Y., Russell, J.M., Linsley, B.K., 2010.
1053 Coordinated hydrological regimes in the Indo-Pacific region during the past
1054 two millennia. Paleoceanography 25, PA1102.
1055 https://doi.org/10.1029/2009PA001871
1056 Ummenhofer, C.C., D'Arrigo, R.D., Anchukaitis, K.J., Buckley, B.M., Cook, E.R.,
1057 2013. Links between Indo-Pacific climate variability and drought in the
1058 Monsoon Asia Drought Atlas. Clim. Dyn. 40, 1319–1334.
1059 https://doi.org/10.1007/s00382-012-1458-1
1060 Vanghi, V., Iriarte, E., Aranburu, A., 2015. High Resolution X-Ray Computed
1061 Tomography for Petrological Characterization of Speleothems. J. Cave Karst
1062 Stud. 77, 75–82.
1063 Vickery, M., 1998. Society, economics, and politics in pre-Angkor Cambodia: the
1064 7th-8th centuries. Cent. East Asian Cult. Stud.
1065 Waibel, H., Pahlisch, T.H., Völker, M., 2018. Farmers' Perceptions of and
1066 Adaptations to Climate Change in Southeast Asia: The Case Study from

1067 Thailand and Vietnam, in: Climate Smart Agriculture, Natural Resource
1068 Management and Policy. Springer, Cham, pp. 137–160.
1069 https://doi.org/10.1007/978-3-319-61194-5_7
1070 Walczak, I.W., Baldini, J.U.L., Baldini, L.M., McDermott, F., Marsden, S., Standish,
1071 C.D., Richards, D.A., Andreo, B., Slater, J., 2015. Reconstructing high-
1072 resolution climate using CT scanning of unsectioned stalagmites: A case study
1073 identifying the mid-Holocene onset of the Mediterranean climate in southern
1074 Iberia. Quat. Sci. Rev., Novel approaches to and new insights from
1075 speleothem-based climate reconstructions 127, 117–128.
1076 https://doi.org/10.1016/j.quascirev.2015.06.013
1077 Wang, J.K., Johnson, K.R., Borsato, A., Amaya, D.J., Griffiths, M.L., Henderson,
1078 G.M., Frisia, S., Mason, A., 2019. Hydroclimatic variability in Southeast Asia
1079 over the past two millennia. Earth Planet. Sci. Lett. 525, 115737.
1080 https://doi.org/10.1016/j.epsl.2019.115737
1081 Wang, Y., Cheng, H., Edwards, R.L., He, Y., Kong, X., An, Z., Wu, J., Kelly, M.J.,
1082 Dykoski, C.A., Li, X., 2005. The Holocene Asian Monsoon: Links to Solar
1083 Changes and North Atlantic Climate. Science 308, 854–857.
1084 https://doi.org/10.1126/science.1106296
1085 Wang, Y.J., 2001. A High-Resolution Absolute-Dated Late Pleistocene Monsoon
1086 Record from Hulu Cave, China. Science 294, 2345–2348.
1087 https://doi.org/10.1126/science.1064618
1088 Wang, Y.J., Cheng, H., Edwards, R.L., An, Z.S., Wu, J.Y., Shen, C.-C., Dorale, J.A.,
1089 2001. A High-Resolution Absolute-Dated Late Pleistocene Monsoon Record
1090 from Hulu Cave, China. Science 294, 2345–2348.
1091 https://doi.org/10.1126/science.1064618
1092 Wedepohl, K.H., 1995. The composition of the continental crust. Geochim.
1093 Cosmochim. Acta 59, 1217–1232. https://doi.org/10.1016/0016-
1094 7037(95)00038-2
1095 Wei, Z., Lee, X., Liu, Z., Seeboonruang, U., Koike, M., Yoshimura, K., 2018.
1096 Influences of large-scale convection and moisture source on monthly
1097 precipitation isotope ratios observed in Thailand, Southeast Asia. Earth Planet.
1098 Sci. Lett. 488, 181–192. https://doi.org/10.1016/j.epsl.2018.02.015
1099 Wohlfarth, B., Higham, C., Yamoah, K.A., Chabangborn, A., Chawchai, S.,
1100 Smittenberg, R.H., 2016. Human adaptation to mid- to late-Holocene climate
1101 change in Northeast Thailand. The Holocene 26, 1875–1886.
1102 https://doi.org/10.1177/0959683616645947
1103 Wong, C.I., Breecker, D.O., 2015. Advancements in the use of speleothems as climate
1104 archives. Quat. Sci. Rev., Novel approaches to and new insights from
1105 speleothem-based climate reconstructions 127, 1–18.
1106 https://doi.org/10.1016/j.quascirev.2015.07.019
1107 Wurtzel, J.B., Abram, N.J., Lewis, S.C., Bajo, P., Hellstrom, J.C., Troitzsch, U.,
1108 Heslop, D., 2018. Tropical Indo-Pacific hydroclimate response to North
1109 Atlantic forcing during the last deglaciation as recorded by a speleothem from
1110 Sumatra, Indonesia. Earth Planet. Sci. Lett. 492, 264–278.
1111 https://doi.org/10.1016/j.epsl.2018.04.001
1112 Xu, C., Buckley, B.M., Promchote, P., Wang, S.-Y.S., Pumijumnong, N., An, W.,
1113 Sano, M., Nakatsuka, T., Guo, Z., 2019. Increased Variability of Thailand's
1114 Chao Phraya River Peak Season Flow and Its Association With ENSO
1115 Variability: Evidence From Tree Ring δ18O. Geophys. Res. Lett. 46, 4863–
1116 4872. https://doi.org/10.1029/2018GL081458

1117 Yamoah, K., Chabangborn, A., Chawchai, S., Schenk, F., Wohlfarth, B., Smittenberg,
1118 R.H., 2016a. A 2000-year leaf wax-based hydrogen isotope record from
1119 Southeast Asia suggests low frequency ENSO-like teleconnections on a
1120 centennial timescale. Quat. Sci. Rev. 148, 44–53.
1121 https://doi.org/10.1016/j.quascirev.2016.07.002
1122 Yamoah, K., Chabangborn, A., Chawchai, S., Väliranta, M., Wohlfarth, B.,
1123 Smittenberg, R.H., 2016b. Large variability in n-alkane δ13C values in Lake
1124 Pa Kho (Thailand) driven by wetland wetness and aquatic productivity. Org.
1125 Geochem. 97, 53–60. https://doi.org/10.1016/j.orggeochem.2016.04.008
1126 Yan, H., Sun, L., Oppo, D.W., Wang, Y., Liu, Z., Xie, Z., Liu, X., Cheng, W., 2011.
1127 South China Sea hydrological changes and Pacific Walker Circulation
1128 variations over the last millennium. Nat. Commun. 2, 293.
1129 https://doi.org/10.1038/ncomms1297
1130 Yan, H., Wei, W., Soon, W., An, Z., Zhou, W., Liu, Z., Wang, Y., Carter, R.M., 2015.
1131 Dynamics of the intertropical convergence zone over the western Pacific
1132 during the Little Ice Age. Nat. Geosci. 8, 315–320.
1133 https://doi.org/10.1038/ngeo2375
1134 Yang H., Johnson K. R., Griffiths M. L., Yoshimura K., 2016. Interannual controls on
1135 oxygen isotope variability in Asian monsoon precipitation and implications for
1136 paleoclimate reconstructions. J. Geophys. Res. Atmospheres 121, 8410–8428.
1137 https://doi.org/10.1002/2015JD024683
1138 Zhang, P., Cheng, H., Edwards, R.L., Chen, F., Wang, Y., Yang, X., Liu, Jian, Tan,
1139 M., Wang, X., Liu, Jinghua, An, C., Dai, Z., Zhou, J., Zhang, D., Jia, J., Jin,
1140 L., Johnson, K.R., 2008. A Test of Climate, Sun, and Culture Relationships
1141 from an 1810-Year Chinese Cave Record. Science 322, 940–942.
1142 https://doi.org/10.1126/science.1163965
1143 Zhou, H., Chi, B., Lawrence, M., Zhao, J., Yan, J., Greig, A., Feng, Y., 2008. High-
1144 resolution and precisely dated record of weathering and hydrological
1145 dynamics recorded by manganese and rare-earth elements in a stalagmite from
1146 Central China. Quat. Res. 69, 438–446. https://doi.org/doi: DOI:
1147 10.1016/j.yqres.2008.02.005
1148 Zisu, N.S., Schwarcz, H.P., Konyer, N., Chow, T., Noseworthy, M.D., 2012.
1149 Macroholes in stalagmites and the search for lost water. J. Geophys. Res.
1150 Earth Surf. 117, F03020. https://doi.org/10.1029/2011JF002288
1151

Figure 1

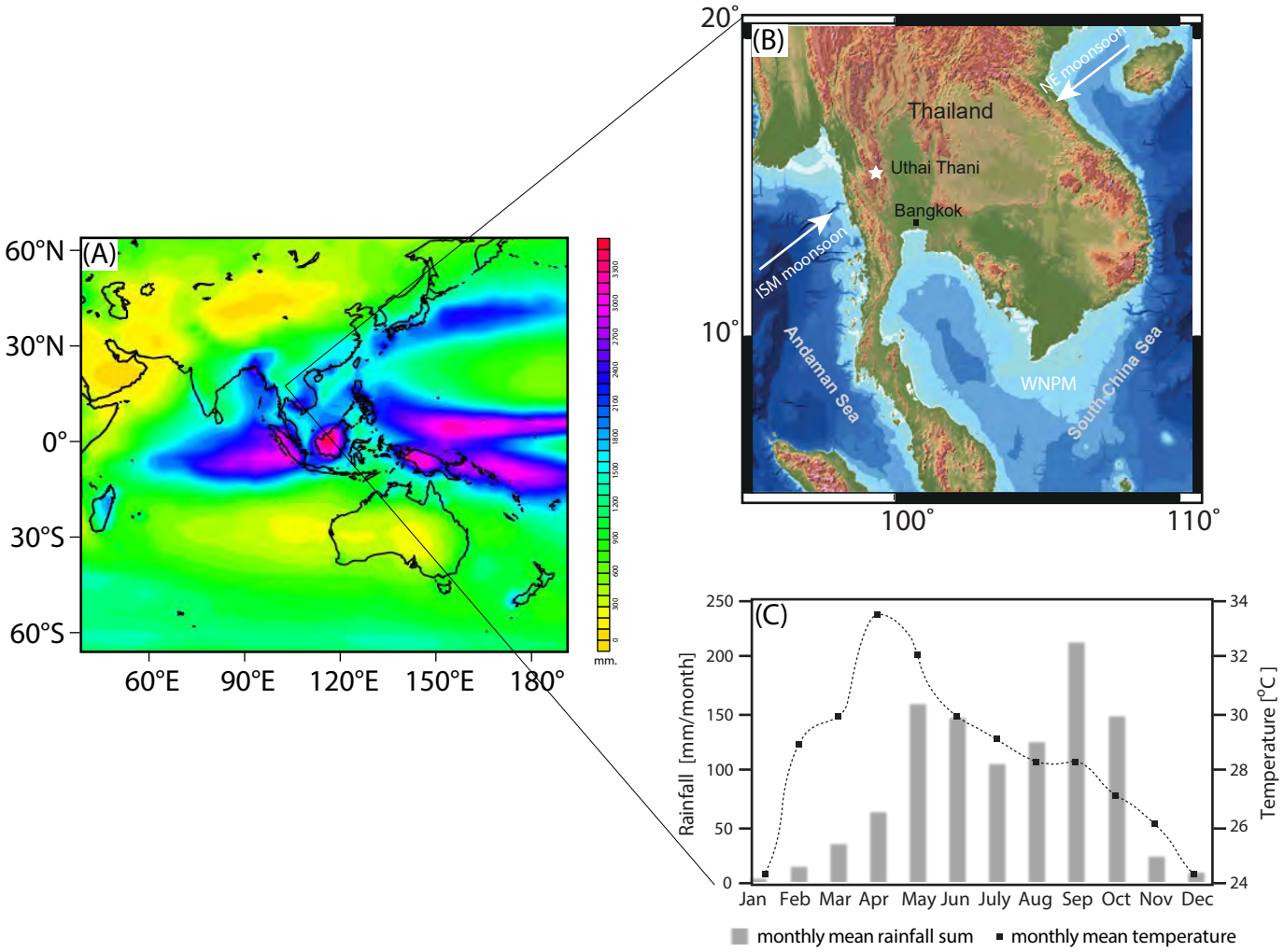
(A)
60°N
30°N
0°
30°S
60°S
60°E
90°E
120°E
150°E
180°
mm.
(B)
20°
10°
100°
110°
Thailand
Uthai Thani
Bangkok
NE moonsoon
ISM moonsoon
Andaman Sea
WNPM
South China Sea
(C)
Rainfall [mm/month]
Temperature [°C]
Jan Feb Mar Apr May Jun July Aug Sep Oct Nov Dec
monthly mean rainfall sum
monthly mean temperature

Figure 4

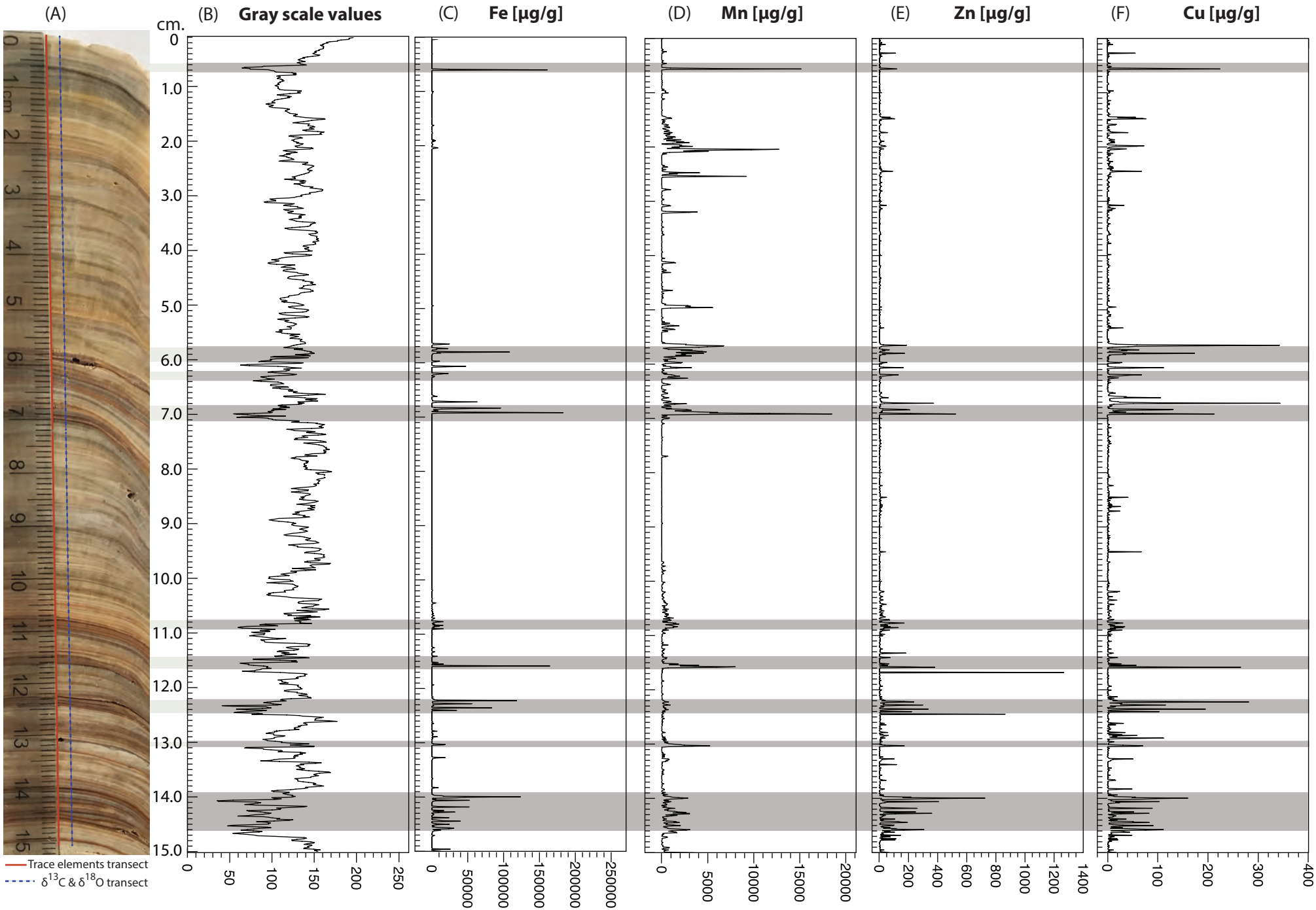
(A)
(B) Gray scale values
(C) Fe [µg/g]
(D) Mn [µg/g]
(E) Zn [µg/g]
(F) Cu [µg/g]
cm.
Trace elements transect
δ13C & δ18O transect

Figure 5

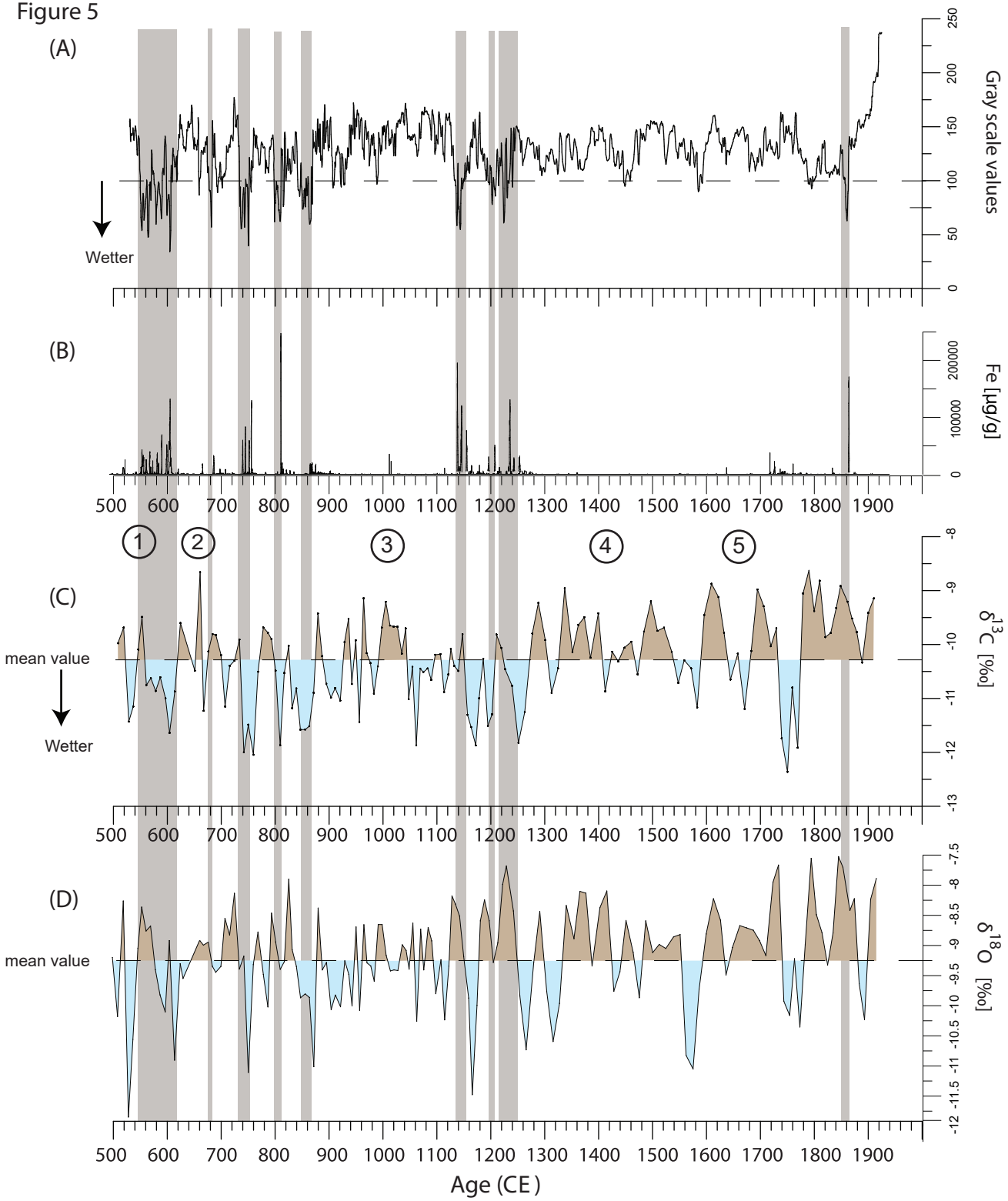

Legends

Higher trace elements intervals

Timing of cultural developments in Mainland Southeast Asia

1. Late Iron age phase 3-4 (200-600 CE)

   abandon moat sites in NE Thailand and move south to new center (500-550 CE)

2. Chenla / Dvaravati States (550-800 CE)

   The power of Chenla break down (700-800 CE)

3. Florescence of Kingdoms in Mainland Southeast Asia (800-1200 AD)

   Khmer / Angkor empires
   (Cambodia, Laos, Thailand, Vietnam)
   Pagan (Myanmar)
   Dai Viet (Vietnam)

4. Angkor empires's demise (1300-1500 CE)

   strong development of Siam Kingdoms (central Thailand) since 1432

5. European colonisation in Southeast Asia (since 1600 CE)

Figure 6

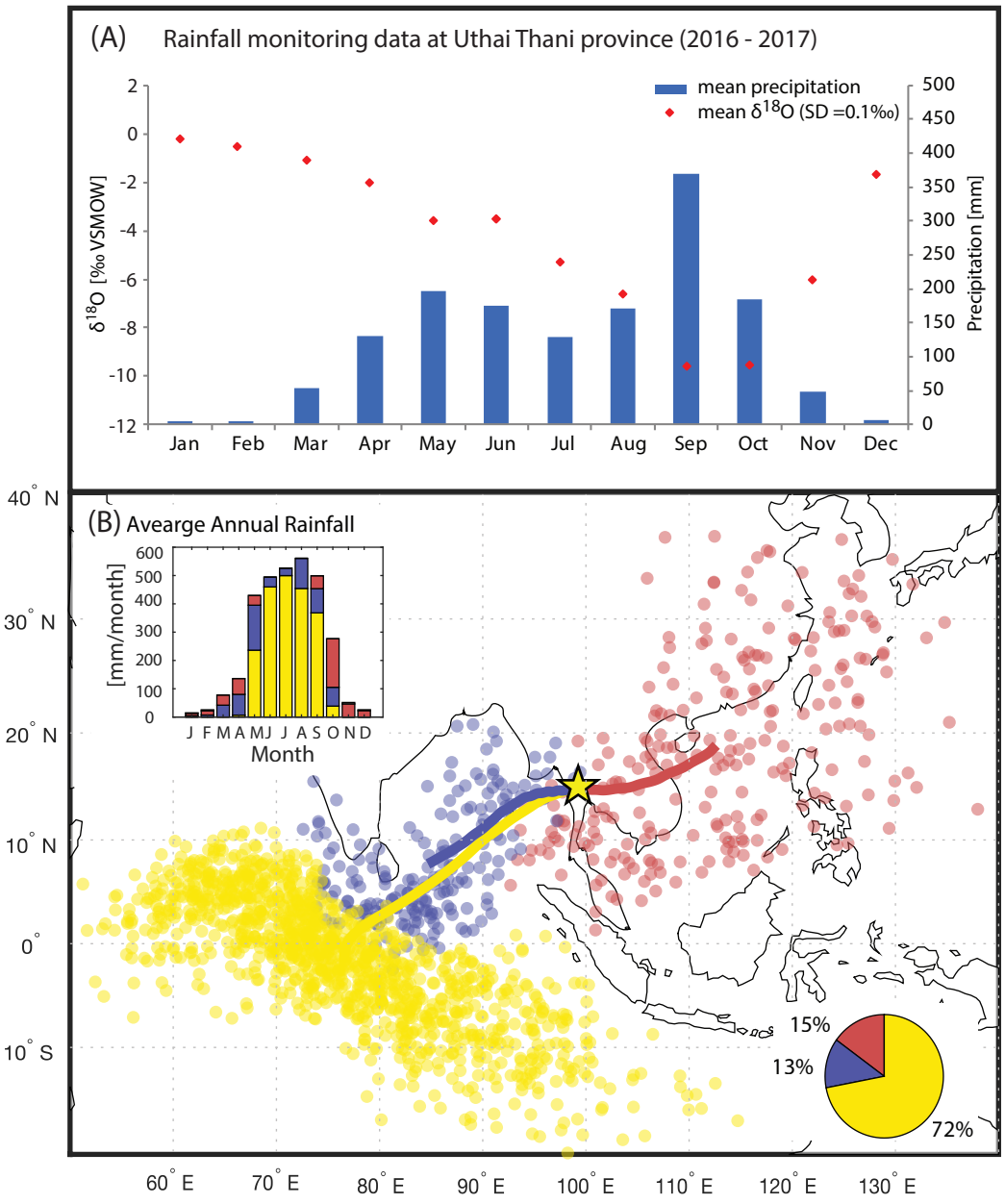
(A) Rainfall monitoring data at Uthai Thani province (2016 - 2017)
mean precipitation
mean δ18O (SD =0.1‰)
δ18O [‰ VSMOW]
Precipitation [mm]
Jan
Feb
Mar
Apr
May
Jun
Jul
Aug
Sep
Oct
Nov
Dec
(B) Avearge Annual Rainfall
[mm/month]
J F M A M J J A S O N D
Month
15%
13%
72%
40° N
30° N
20° N
10° N
0°
10° S
60° E
70° E
80° E
90° E
100° E
110° E
120° E
130° E

Figure 7

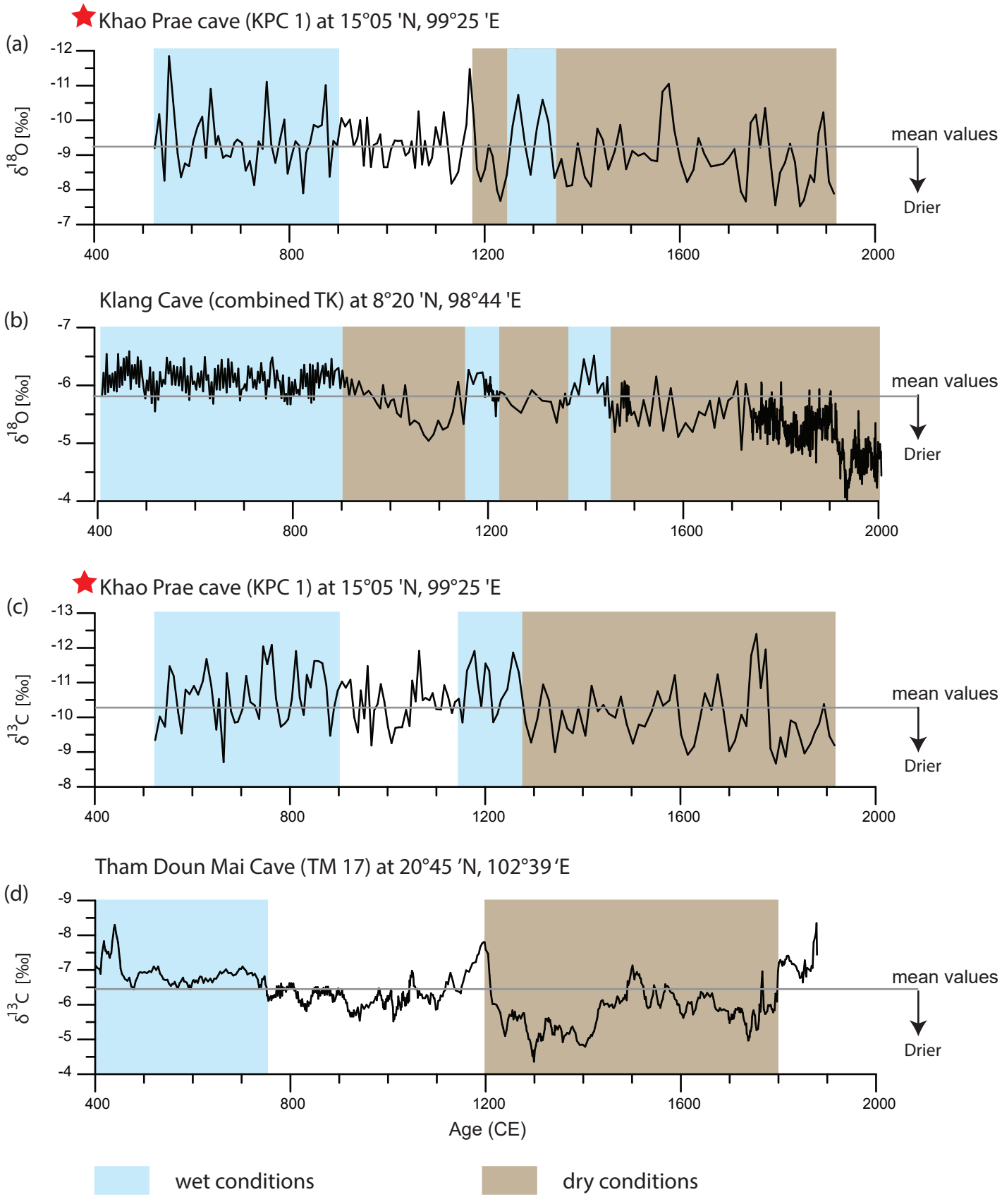
Khao Prae cave (KPC 1) at 15°05 'N, 99°25 'E
(a)
δ18O [‰]
-12
-11
-10
-9
-8
-7
400
800
1200
1600
2000
mean values
Drier
Klang Cave (combined TK) at 8°20 'N, 98°44 'E
(b)
δ18O [‰]
-7
-6
-5
-4
400
800
1200
1600
2000
mean values
Drier
Khao Prae cave (KPC 1) at 15°05 'N, 99°25 'E
(c)
δ13C [‰]
-13
-12
-11
-10
-9
-8
400
800
1200
1600
2000
mean values
Drier
Tham Doun Mai Cave (TM 17) at 20°45 'N, 102°39 'E
(d)
δ13C [‰]
-9
-8
-7
-6
-5
-4
400
800
1200
1600
2000
Age (CE)
mean values
Drier
wet conditions
dry conditions

Figure 8

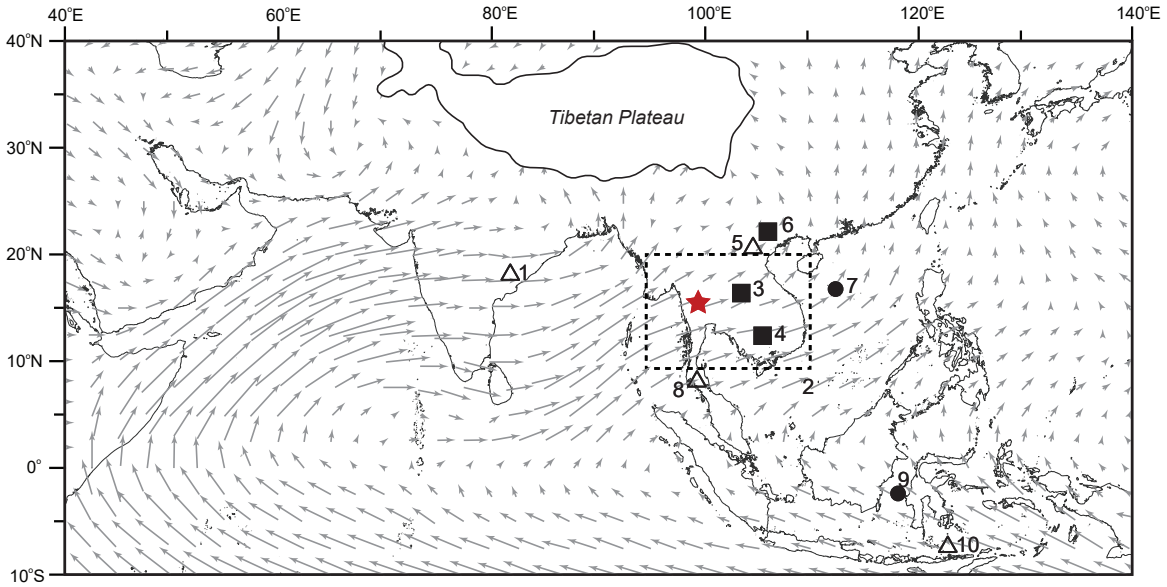

Legends

- Marine records
- Speleothem $\delta^{18}O$ records
- KPC1 This study
- Lake/resevoir records
- Tree-ring data SE Asia
- Wetter condition
- Drier condition

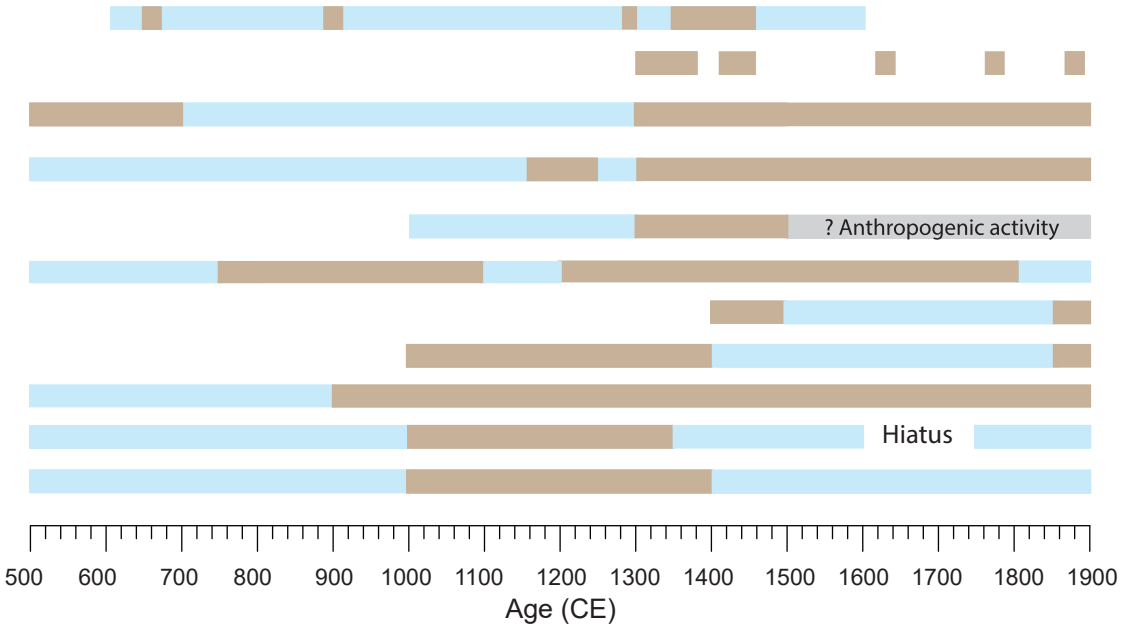

(1) Dandak cave
(2) Tree-ring SE Asia
(3) Lake Pa Kho
KPC1
(4) Angkor Wat resevoir
(5) Tham Doun Mai cave
(6) Lake Ao Tiên
(7) Cattle pond
(8) Klang cave
(9) SW Sulawesi
(10) Liang Luar cave